Available online at www.sciencedirect.com
SCIENCE DIRECT®
Earth and Planetary Science Letters 240 (2005) 11–72
EPSL
www.elsevier.com/locate/epsl

Stratigraphy and sedimentology of a dry to wet eolian depositional system, Burns formation, Meridiani Planum, Mars

J.P. Grotzinger [a,*], R.E. Arvidson [b], J.F. Bell III [c], W. Calvin [d], B.C. Clark [e], D.A. Fike [a], M. Golombek [f], R. Greeley [g], A. Haldemann [f], K.E. Herkenhoff [h], B.L. Jolliff [b], A.H. Knoll [i], M. Malin [j], S.M. McLennan [k], T. Parker [e], L. Soderblom [g], J.N. Sohl-Dickstein [b], S.W. Squyres [b], N.J. Tosca [k], W.A. Watters [a]

[a] *Massachusetts Inst. of Technology, Earth, Atmos. and Planetary Sci., Cambridge, MA 02139, USA*
[b] *Department Earth and Planetary Sciences, Washington University, St. Louis, MO 63130, USA*
[c] *Department of Astronomy, Space Sciences Bldg. Cornell University, Ithaca, NY 14853, USA*
[d] *University of Nevada, Reno, NV 89501, USA*
[e] *Lockheed Martin Corporation, Littleton, CO 80127, USA*
[f] *Jet Propulsion Laboratory, California Institute of Technology, Pasadena, CA 91109, USA*
[g] *Department Geological Sciences, Arizona State University, Box 871404, Tempe, AZ 85287-1404, USA*
[h] *U.S. Geological Survey, Flagstaff, AZ 86001, USA*
[i] *Botanical Museum, Harvard University, Cambridge MA 02138, USA*
[j] *Malin Space Science Systems, Inc., San Diego, CA 92191, USA*
[k] *Department of Geosciences, State University of New York, Stony Brook, NY 11794-2100, USA*

Accepted 22 September 2005

Editor: A.N. Halliday

Abstract

Outcrop exposures of sedimentary rocks at the Opportunity landing site (Meridiani Planum) form a set of genetically related strata defined here informally as the Burns formation. This formation can be subdivided into lower, middle, and upper units which, respectively, represent eolian dune, eolian sand sheet, and mixed eolian sand sheet and interdune facies associations. Collectively, these three units are at least 7 m thick and define a "wetting-upward" succession which records a progressive increase in the influence of groundwater and, ultimately, surface water in controlling primary depositional processes.

The Burns lower unit is interpreted as a dry dune field (though grain composition indicates an evaporitic source), whose preserved record of large-scale cross-bedded sandstones indicates either superimposed bedforms of variable size or reactivation of lee-side slip faces by episodic (possibly seasonal) changes in wind direction. The boundary between the lower and middle units is a significant eolian deflation surface. This surface is interpreted to record eolian erosion down to the capillary fringe of the water table, where increased resistance to wind-induced erosion was promoted by increased sediment cohesiveness in the capillary fringe. The overlying Burns middle unit is characterized by fine-scale planar-laminated to low-angle-stratified sandstones. These sandstones accumulated during lateral migration of eolian impact ripples over the flat to gently undulating sand sheet surface. In terrestrial settings, sand sheets may form an intermediate environment between dune fields and interdune or playa surfaces. The contact between the middle and upper units of the Burns formation is interpreted as a diagenetic front, where recrystallization in the

* Corresponding author. Permanent address: Division of Geological and Planetary Sciences, California Institute of Technology, Pasadena, CA 91125, USA. Tel.: +1 626 395 6785; fax: +1 626 568 0935.
E-mail address: grotz@gps.caltech.edu (J.P. Grotzinger).

0012-821X/$ - see front matter
doi:10.1016/j.epsl.2005.09.039

phreatic or capillary zones may have occurred. The upper unit of the Burns formation contains a mixture of sand sheet facies and interdune facies. Interdune facies include wavy bedding, irregular lamination with convolute bedding and possible small tepee or salt-ridge structures, and cm-scale festoon cross-lamination indicative of shallow subaqueous flows marked by current velocities of a few tens of cm/s. Most likely, these currents were gravity-driven, possibly unchannelized flows resulting from the flooding of interdune/playa surfaces. However, evidence for lacustrine sedimentation, including mudstones or in situ bottom-growth evaporites, has not been observed so far at Eagle and Endurance craters.

Mineralogical and elemental data indicate that the eolian sandstones of the lower and middle units, as well as the subaqueous and eolian deposits of the Burns upper unit, were derived from an evaporitic source. This indirectly points to a temporally equivalent playa where lacustrine evaporites or ground-water-generated efflorescent crusts were deflated to provide a source of sand-sized particles that were entrained to form eolian dunes and sand sheets. This process is responsible for the development of sulfate eolianites at White Sands, New Mexico, and could have provided a prolific flux of sulfate sediment at Meridiani. Though evidence for surface water in the Burns formation is mostly limited to the upper unit, the associated sulfate eolianites provide strong evidence for the critical role of groundwater in controlling sediment production and stratigraphic architecture throughout the formation.

Keywords: Mars; Meridiani; sedimentology; environmental history; stratigraphy; eolian

1. Introduction

Historical accounts of planetary evolution are mostly written in stone. The chemical diversity of igneous rocks and meteorites, crater impact chronologies, and the geomorphic character of planetary and lunar surfaces provide a few examples of records that constrain fundamental processes and events in planetary evolution. In addition, any process that operates at a planetary surface has the potential to create a record of sedimentary rocks. This is important because our experience on Earth shows that sediments and sedimentary rocks preserve high-resolution proxies of present and past tectonic, climatic, and biological processes as well as providing the dominant archive of major events in Earth's evolution. Sedimentary rocks precipitated from water are particularly important because they embed signals of elemental and isotopic variability that relate to geochemical and biogeochemical processes, expressed at local to global scales.

Past observations from orbit of sedimentary rocks on Mars [1] that may have been formed in water [2] provide encouragement that high-resolution records of environmental and possibly biologic processes may be preserved. The Mars Exploration Rover Opportunity confirms this expectation with its discovery of stratified sedimentary rocks at Meridiani Planum, which is remarkable for several reasons. To begin with, some of these rocks formed in water and all of them were altered by water [3–8]. This confirms earlier, mostly geomorphic evidence for the existence of liquid water on the surface of Mars in the geologic past [9]. In turn, it helps motivate future missions to Mars designed to search for evidence of past life [10]. However, the discovery of sedimentary rocks at Meridiani also is exciting because it establishes an unprecedented access point to begin the characterization and interpretation of the first high-resolution records of Martian history. Earth's ancient sedimentary record can preserve signals of variability on a time scale of 10^3–10^5 yrs–important, say, for interpreting climate change–depending on the interplay of the dynamic variables that control stratigraphic architecture: tectonic subsidence rate, changes in base level, and the flux of sediment [11,12]. These variables control the spatial partitioning of sediment volumes and the magnitude and frequency of omission surfaces that separate those volumes. If stratified sedimentary rocks are viewed as the carrier signal for proxies of planetary evolution, then these variables are what control the fidelity of that signal.

Data returned by Opportunity allow a first pass at evaluating this signal of Martian history. In principle, the stratigraphic architecture of sedimentary rocks on Mars must be similar to Earth in at least a general way owing to the constancy of basic physical principles that describe the behavior of fluids and solids, and the conservation of mass and energy. The extended life of Opportunity has resulted in a remarkable discovery: that not only are the patterns generally similar, they are similar in detail. This surprising coherence leads to formulation of a predictive depositional model based on sedimentologic analysis of primary and diagenetic facies, the stratigraphic distribution of facies in space and time, and the construction a broader environmental framework from which to interpret the early history of Mars.

2. Regional setting

The Opportunity landing site is located within the classical low-albedo region Sinus Meridiani (Figs. 1 and 2), which straddles the Martian Prime Meridian from 10°W to 10°E longitude, 13°S to 7°N latitude. This region was selected as a landing site primarily because orbital observations by the Mars Global Surveyor Thermal Emission Spectrometer indicated an anomalous concentration of hematite [13,14]. The low-albedo surface materials are superposed on an eroded, light-toned, layered substrate that approaches 1 km thickness in northern Sinus Meridiani, and which overlies (unconformably?) exhumed, partly eroded cratered terrain in southern Sinus Meridiani (Fig. 1). Prior to Opportunity's surface investigations, the layered units beneath and north of the Opportunity landing site had been interpreted as a possible eolian mantle and/or volcanic plain [15–17], a paleopolar layered deposit [18], a subaqueous sedimentary deposit [19], and sedimentary rocks reflecting a variety of depositional environments [1,13,14,20]. The hematite enrichment was attributed to enhanced precipitation from Fe-rich fluids. However, the hematite is now known to be associated with a lag deposit of hematitic granules [21] released during the physical breakdown of a sedimentary bedrock containing a few percent by volume hematitic concretions [3,7,22].

At kilometer scales, three distinct geomorphic expressions reflect the basic rock types within the Meridiani region: (1) a cratered terrain, characterized by a high abundance of 1–10 km diameter craters; (2) nearly uncratered, light-toned layered sedimentary rock units that have "massive" and "stair-stepped" outcrop patterns; and (3) relatively dark, smooth or ridged-and-grooved mantles which overprint the previous two geomorphic types. Mapping of these geomorphic types, in particular in northern Meridiani, suggests broad distribution of at least four major rock-stratigraphic units, each 200–300 m thick, exposed by erosion [23]. Unconformities between these units, marked in part by interbedded craters with diameters of up to 60 km, attest to substantial hiatuses between deposition of stratigraphically contiguous units. Lateral continuity of layering for distances in excess of 100 km demonstrates the essentially horizontal attitude of these strata. The exact relationship between these units and the light-toned sedimentary rocks at the Opportunity landing site (Burns formation, see below) seen hundreds of kilometers to the south is difficult to determine due to the

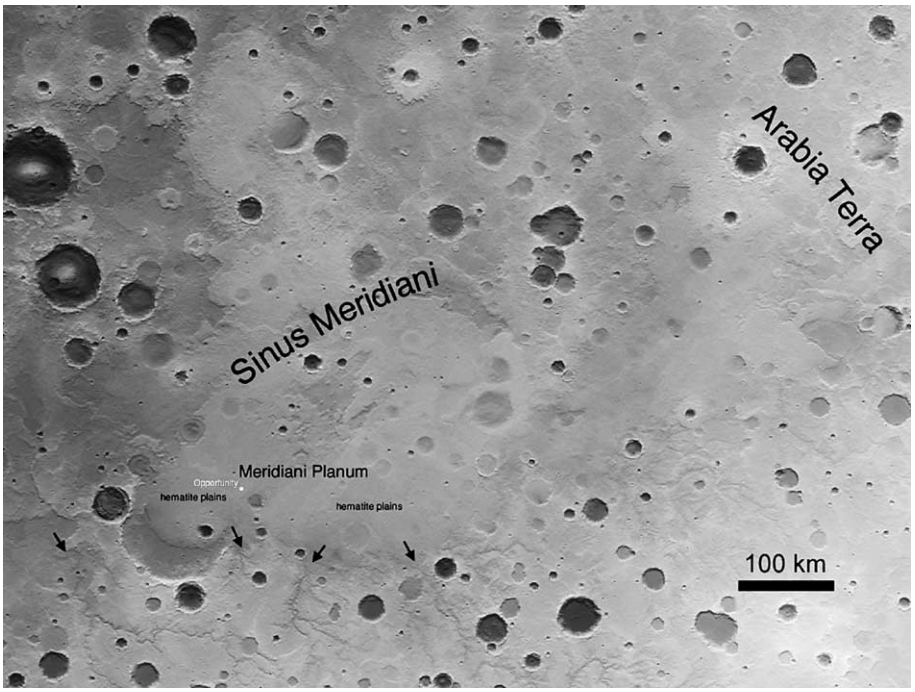

Fig. 1. Location of Opportunity landing site in the Meridiani Planum region. A dissected, cratered terrain in the southern part of image is overlain (unconformably?) by younger, layered, sedimentary rocks. The arrows point to the contact which separates these two geologic units. Note differences in surface morphology, which reflect underlying geologic units. See text for further discussion. The image combines the 128 pixel per degree Mars Orbiter Laser Altimeter (MOLA) gridded altimetry product (bright is higher, dark is lower) with shaded relief illuminated from the north.

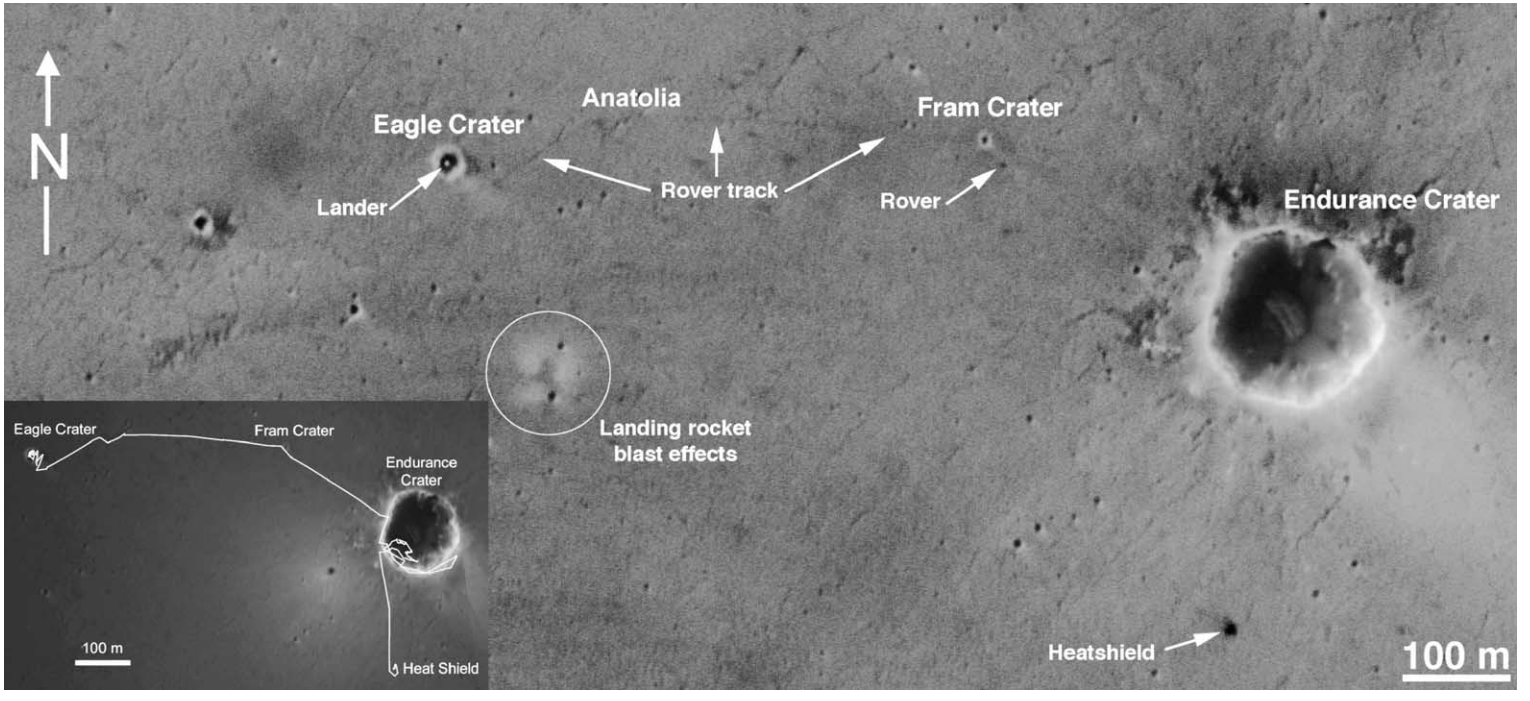

Fig. 2. Mars Orbiter Camera (MOC) compensated pitch and roll targeted observation (cPROTO) image (0.5 m/pixel) of the Opportunity landing area and rover path. This image is a sub-frame of MOC image R16-02188. It was acquired on 26 April 2004, during Opportunity's 91st sol, when the rover was enroute toward Endurance Crater. The rover itself can be seen in this image, and some segments of its tracks are just visible. The lander is visible in Eagle crater. Sunlight illuminates the scene from the left, the scale bar is 100 m and north is toward the top. The inset shows the complete rover traverse path as of sol 352, when it had circumnavigated the heat shield. Note the loop within the crater: the image of Burns Cliff shown in Fig. 4 was obtained from the easternmost point in this loop, looking toward the southeast. Image credit: NASA/JPL/MSSS.

masking effects of the basaltic sand and hematitic granule veneer. However, the available data, including underlying rock units and their relationship to local and regional topography suggest that the Burns formation represents a stratigraphic level which is equivalent to the lower part of the topmost rock-stratigraphic unit in northern Meridiani.

The local vicinity of the Opportunity landing site is characterized by an extremely flat, uniform plain (Fig. 2). North of the landing site, NE/SW-trending fractures (Fig. 2) and small impact craters are relatively abundant, but the fractures disappear within a kilometer or so south of the landing site, and the number of impact craters drops dramatically. Commensurate with these southward changes, the plains surface slopes upward very gently and the surface is covered by a veneer of eolian ripples and dunes that creates a small-scale ridge-and-groove morphology. These eolian bedforms grow in amplitude from a few cm near Endurance crater to several tens of cm near Erebus crater, a few km south of Endurance. In the vicinity of Erebus crater the small-scale ridge-and-groove morphology gives way to a larger-scale ridge-and-groove morphology. Even farther south, this terrain merges with a higher-standing smooth plain. These geomorphic changes, combined with the regionally horizontal attitude of larger-scale layered units, suggest that the plain follows a prominent stratigraphic contact (potentially a sequence boundary or significant facies change) and that the overlying strata, perhaps more easily eroded, have been mostly removed from the site. Total relief within 10 km of the landing site varies by little more than 10 m, suggesting that the overlying stratigraphic interval was approximately as thick as the strata which define the Burns formation in Endurance crater.

3. Stratigraphy

3.1. Burns formation

The term “Burns formation” is introduced to include all of the rocks explored by Opportunity that occur in bedrock exposures created as a result of impact-related crater formation (Eagle, Fram, Endurance), or regional fracturing (Anatolia). This informal name honors Roger Burns, who predicted on the basis of Viking chemistry that ferric sulfate minerals–including jarosite–should occur and be stable on the surface of Mars [24]. The name is derived from Burns Cliff, a feature in Endurance crater where the Burns formation is particularly well exposed. Though the rocks of the Burns formation differ in their sedimentology, having been transported and deposited in both subaqueous and eolian environments, they all fit within the same depositional model. Similarly, the Burns formation contains jarosite at all localities, along with other sulfate minerals including calcium and magnesium sulfates, despite local changes in elemental abundance [4,6,8]. Thus, the term “Burns formation” describes a group of rocks which likely consists of a genetically related set of strata, with specific textural, sedimentologic, and geochemical attributes, and which can be minimally mapped across the area of the landing site and has a thickness of at least 10 m. On the basis of MOC and TES data [25] it likely extends much farther and is also much thicker than has been observed so far.

3.2. Stratigraphic framework

Outcrops of the Burns formation were examined at Eagle crater, the Anatolia fracture network, Fram crater, and Endurance crater. The heights of exposed outcrops are 30–50 cm at Eagle and 10–20 cm at Anatolia and Fram. Endurance crater exposes at least 7 m of outcrop and thus serves as the principal locality for establishing the stratigraphy of the Burns formation. To obtain true stratigraphic thicknesses, one must be able to correct for deformation of strata associated with folding, faulting, and brecciation due to impact. At Eagle, Anatolia, and Fram the bedrock is fractured and consists of rotated blocks. In general, systematic deformation patterns are absent, which precludes ordering of the stratigraphy at those locations. Exceptions to this are the El Capitan and Big Bend areas of Eagle crater, where strata can be traced laterally for several meters as mostly intact units [3]. At Endurance crater, a correction was made for the impact-generated structural dip at Burns Cliff to obtain the true stratigraphic thickness of strata beneath the impact breccia layer.

The exposures at the Karatepe and Burns Cliff segments of Endurance crater provide the most insight into the stratigraphic ordering of the Burns formation. Here, the formation is subdivisible into three units (Fig. 3). The lower two units are minimally deformed, showing moderate dip toward the perimeter of the crater (Figs. 4 and 5a). In contrast, much of the upper unit displays extensive brecciation similar to that seen at Eagle and Fram. The three units of the Burns formation are distinguished on the basis of primary sedimentary structures, secondary diagenetic textures, color, and the morphology of the weathered surface. The lower unit is exposed at the base of Burns Cliff and consists of several meters of large-scale cross-bedded sandstone. In addition, this lower unit contains hematitic concretions.

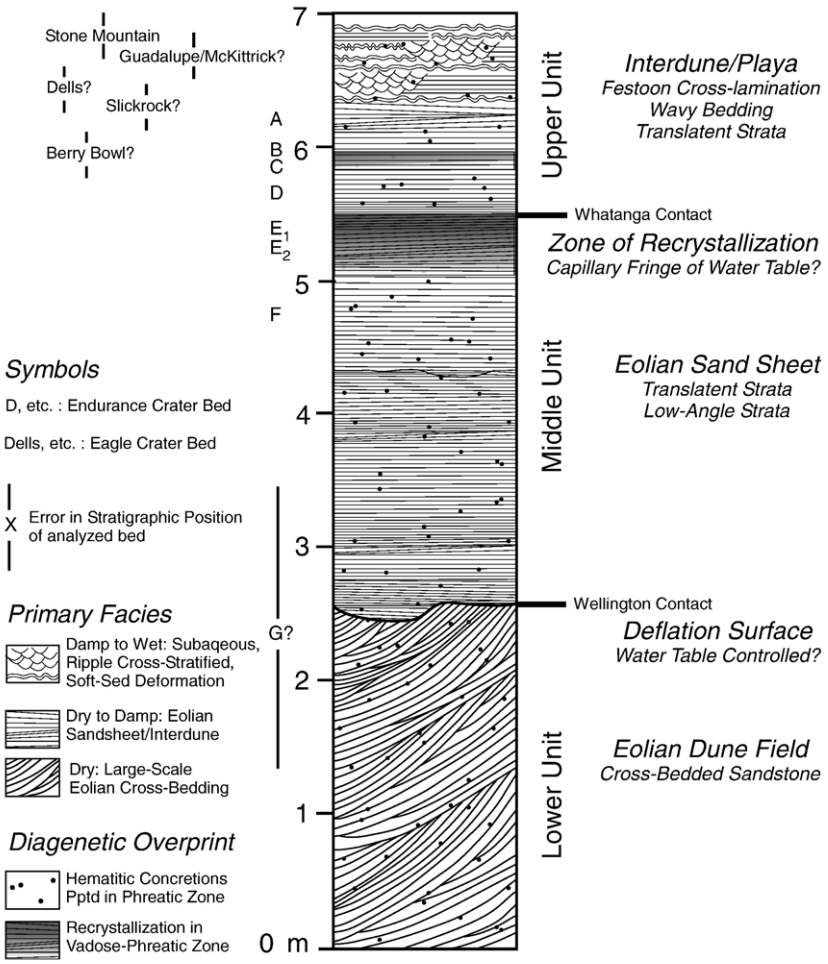

Fig. 3. Stratigraphy of Burns formation. Letters and names on the left side of the stratigraphic column show the likely stratigraphic position of key rocks that are discussed in papers by Clark et al. [8] and McLennan et al. [7]. Three units within the Burns formation are defined based on sedimentologic and diagenetic attributes. The lower unit is composed exclusively of large-scale cross-bedded sandstones and is separated from the overlying middle unit by a disconformable surface (Wellington contact) interpreted as a deflation surface. The middle unit is dominated by planar-stratified to low-angle cross-stratified sandstones interpreted as an eolian sand sheet. Rare subaqueous current-ripple cross-lamination indicate an occasionally damp to wet environment. The contact between the middle and upper units (Whatanga contact) is a diagenetic zone of recrystallization, interpreted to have formed in the capillary fringe of the water table. The upper unit of the Burns formation is composed of both eolian sand sheet and subaqueous interdune facies. Considered collectively, these three units record an upward increase in the involvement of groundwater and surface water in controlling facies and stratigraphic architecture.

This lower unit has a truncated top and is disconformably overlain by the middle unit (Figs. 5b and 6a). The middle unit is dominated by several meters of planar-laminated to low-angle cross-stratified sandstone that also contain hematitic concretions. In addition, the middle unit is characterized by a pervasive overprint of nodular recrystallization, and secondary porosity development. This phase of diagenesis post-dates growth of the hematitic concretions and is expressed by the development of a nodular texture in the rock matrix, the precipitation of overgrowths on the hematitic concretions, and the creation of secondary porosity [7]. Bedding may be nearly massive; however, palimpsest fine lamination often is still visible even in parts of the outcrop with the most intense recrystallization. The contact between the middle and upper units is a diagenetic boundary marked by an abrupt upward decrease in the extent of nodular recrystallization, accompanied by a shift from dark to light color (Figs. 5c and 6b). The contact is placed at the top of the first of several of these darker colored zones. Strata of the upper unit are lighter toned than underlying units and exhibit planar lamination, low-angle stratification, small-scale cross-bedding in sets of up to 10 cm, and rare cm-scale sets of festoon

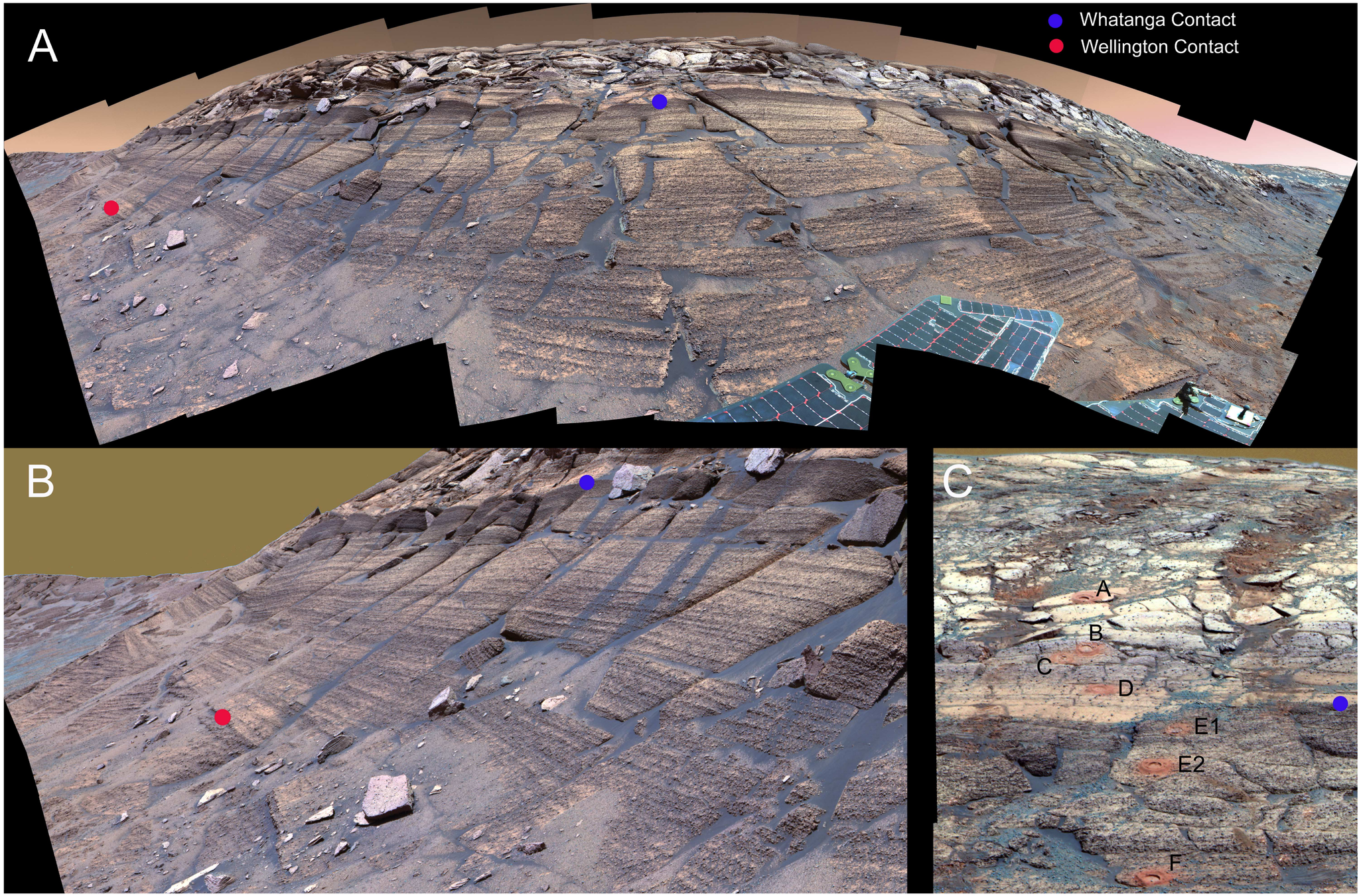

Fig. 4. The Burns formation at Burns cliff, southeast rim of Endurance crater. (a) Complete Burns cliff outcrop. (b) Enlargement of left (East) side of Burns cliff outcrop. The three informal subdivisions ("units") of the formation are visible: lower unit, beneath "Wellington" contact, exposes cross-bedded sandstone; middle unit, above Wellington contact and beneath "Whatanga" contact, exposes planar to low-angle cross-stratified sandstone; upper unit, above Whatanga contact, exposes light-toned eolian and subaqueous facies. Note scour along Wellington contact, and dark tone of rocks beneath Whatanga contact. Compare with Fig. 5a to obtain sense of scale. (c) Exposure at Karatepe showing Whatanga contact, and its position relative to the 7 RAT holes which provide constraints on chemistry and mineralogy (see Clark et al. [8]). The images are all false color composite mosaics. (a) and (b) were generated from images acquired as part of the Opportunity sol 287 to 294 Burns Cliff mosaic, using Pancam's 750, 530, and 430 nm filters, and spanning about 65° in azimuth by about 25° in elevation. (c) was generated using images acquired on Opportunity sol 173.

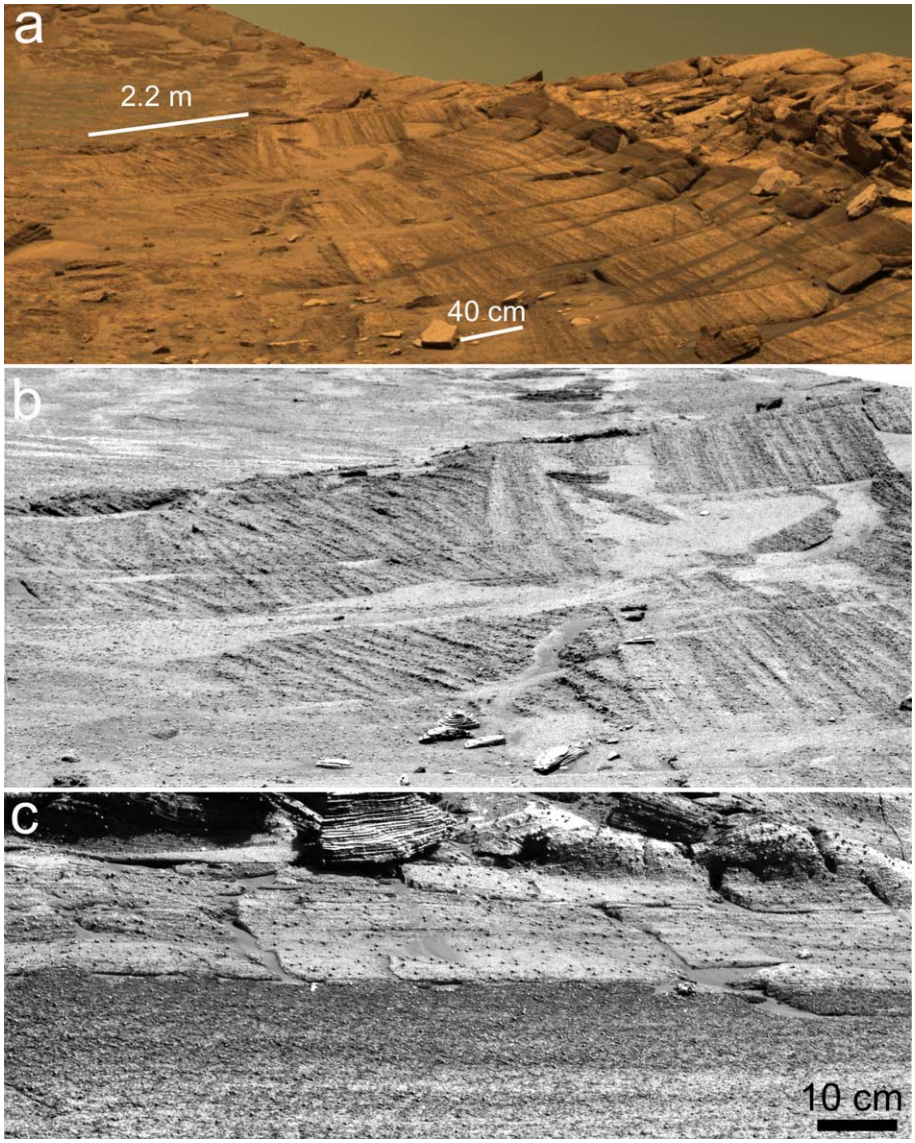

Fig. 5. Contacts between stratigraphic units of the Burns formation as obtained by the Pancam at Burns cliff, Endurance crater. (a) Burns formation at eastern end of Burns cliff. The three informal subdivisions (lower, middle, and upper units) of the formation are visible, as described in Fig. 4. Because of its broad coverage, the scale varies significantly across area of image. This image is an approximate true-color composite mosaic generated from images acquired on sol 278, sequence P2440, using Pancam's 750, 530, and 430 nm filters. (b) Close-up of Wellington contact and Burns lower unit strata. Note thick lamination of cross-bedding below contact, which contrasts with fine lamination above. Scale of cross-bedding provided by bar in (a), and by visible concretions (small black dots) which are up to 3–5 mm in diameter. Grayscale "super-resolution image" using Pancam's 430 nm filter on sol 288. (c) Close-up of Burns middle unit/upper unit transition and Whatanga contact. Contact is characterized by an upward gradation from light to dark tone in upper part of middle unit, followed by an abrupt shift to a much lighter tone which defines the contact. Grayscale "super-resolution image" using Pancam's 430 nm filter on sol 289.

cross-lamination. The thickness of the upper unit is indeterminate due to extensive brecciation of all but the lowermost 10–30 cm, immediately above the contact. This upper unit has been studied in the most detail at Eagle crater where extensive observations were made of primary bedding attributes at the Last Chance, Dells, Slickrock, and Shoemaker's Patio localities [3].

4. Facies and depositional processes

Each stratigraphic unit can be characterized by an assemblage of rock types, or *facies*. As used here, the term facies is used to describe a body of rock characterized by a particular combination of lithology and sedimentary structures that bestow an aspect ("facies")

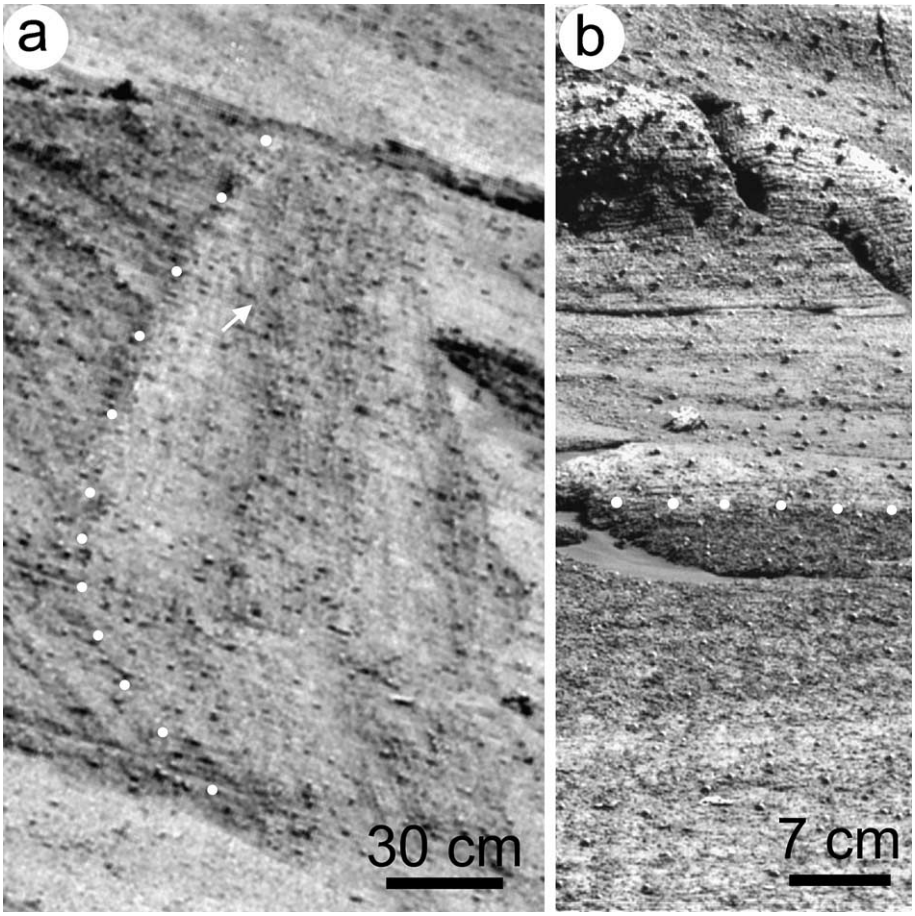

Fig. 6. Enlargement of portions of Fig. 5b and c to show sedimentologic details. (a) Scour and infill along Wellington contact, highlighted by filled white circles. Infill is dominated by fine, planar stratification to low-angle cross-stratification, suggestive of eolian translatent strata formed by migration of eolian impact ripples. Arrow indicates shallow scour approximately 2 cm deep and 5 cm wide developed within infill strata. If the reader rotates the image 90° in a counterclockwise direction several other scour-and-fill features can be seen. Low-angle cross-strata have a net eastward dip. Note also the lack of fine lamination in the cross-bedding beneath the contact, suggesting an origin through grain flow or grain fall. For scale, the mean diameter of the concretions (dark dots) is approximately 4 mm. Grayscale "super-resolution image" using Pancam's 430 nm filter on sol 288. (b) The gradational shift to progressively darker tones marks the upward transition to the Whatanga contact, followed by an abrupt shift to lighter tones above the contact. The contact is highlighted by filled white circles. For scale, the upper size limit of the concretions is approximately 3–5 mm in diameter. Note that the density of concretions is unchanged across the contact, suggesting that the dark band records a subsequent diagenetic event. Compare with another view of the Whatanga contact, Fig. 11a, obtained at Karatepe East. Grayscale "super-resolution image" using Pancam's 430 nm filter on sol 288.

different from the bodies of rock above, below, and laterally adjacent. Each facies records a distinct set of depositional processes.

The Burns formation has several sandstone-dominated facies. Component sand grains likely were derived from reworked, siliciclastic-rich evaporites. Mudstones have not been identified, though it is possible in some cases that recrystallization of evaporite minerals coarsened textures so that primary attributes are now obliterated. However, even in these cases the presence of fine lamination, discussed further below, makes it most likely that these deposits accumulated as a result of bedload traction transport of silt- to sand-sized particles rather than settling of suspended fines.

In the best-preserved examples, the primary grain size of particles is on the order of 0.3 to 0.8 mm, dominated by medium-grained sand (Fig. 7). Coarser particles are not present, though finer particles may have been coarsened due to recrystallization. The grains illustrated in Fig. 7a show a clear variation in size from lamina to lamina suggestive of bimodal sorting, or graded lamination. This texture is common in many Burns outcrops and commonly results in a distinctive "pinstripe" lamination. Such textures are consistent with

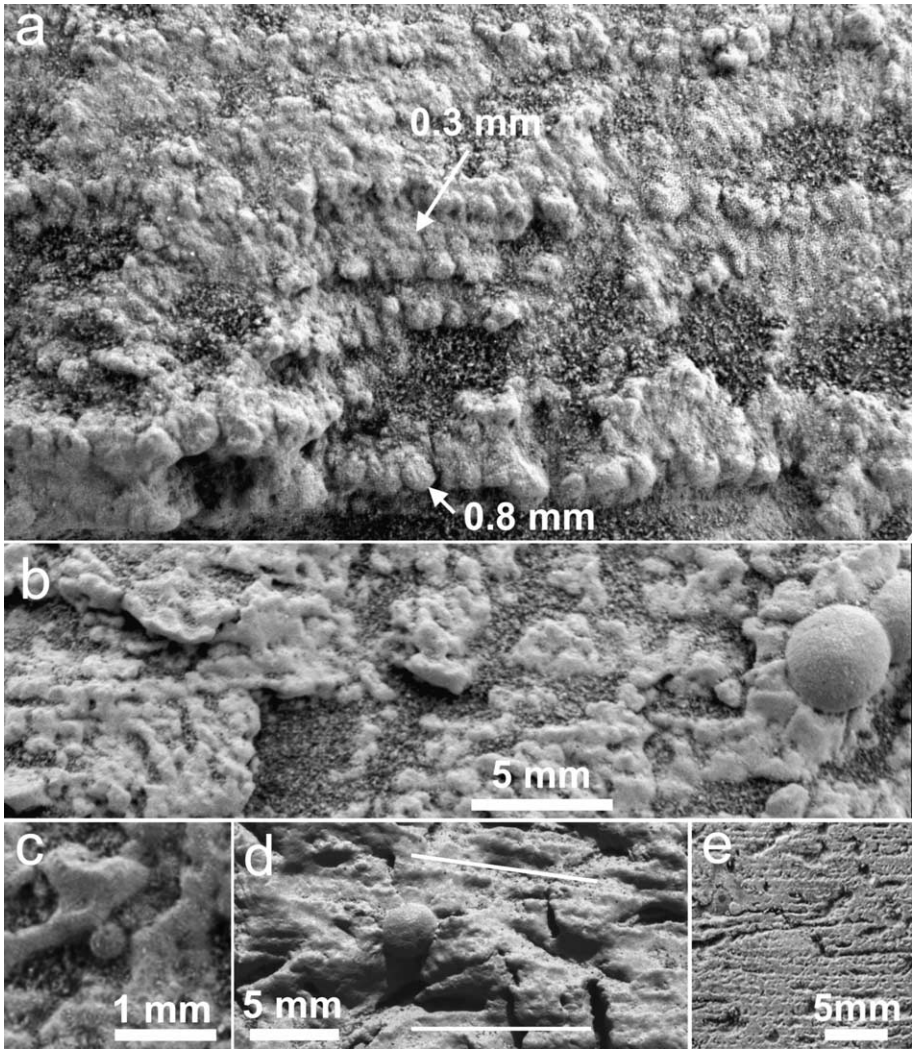

Fig. 7. Grain-scale textures revealed by Microscopic Imager. (a) Distinct grains form lamination ("Flatrock", Eagle crater), indicating that most of the Burns formation was composed of sandstones, whose grains were derived from reworked evaporites. Grains range in size from 0.1 to 1.0 mm, are moderately well rounded, and are well sorted into discrete laminae. The excellent size sorting on the scale of individual laminae is strongly suggestive of "translatent" strata, formed by sediment transport within migrating eolian impact ripples. Fabric preservation which reveals discrete grains is rare due to cementation recrystallization; preservation is best where early cementation was minimal, permitting grains to weather in positive relief. Compare with (b) and (d), which show the effects of increasing cementation. The image (1M131912465) was acquired by the MI on sol 042 with the target in complete shadow. (b) Effects of early cementation and recrystallization are visible in the center left ("Algerita", Eagle crater). Note set of 3 or 4 laminae, expressed by fused grains. The lack of expression of individual grains, as compared to (a), is interpreted to reflect the greater extent of early cementation. At center right, the effects of recrystallization on destruction of primary fabrics are well illustrated by a halo which envelops a hematitic concretion. Note complete loss of primary fabric and development of blocky, interlocking crystals. The image is part of a merge of 5 images (1M130671710 to 1M130672029) that were acquired by the MI on sol 28 with the target in complete shadow. (c) Rare small, spherical grain ("McKittrick", Eagle crater). Part of MI image 1M130670821, taken on sol 28 in complete shadow. (d) Nearly complete early cementation results in loss of grain boundaries ("Guadalupe", Eagle crater). Relict lamination is highlighted by white lines. Compare with (b) and (a). Part of image 1M130761568, acquired by the MI on sol 29; direct illumination from top. (e) Fresh surface produced by the Rock Abrasion Tool reveals fine lamination, including truncated laminae visible at center left ("Kentucky", Endurance crater). Grains are fused due to early cementation, which is concentrated along thicker laminae which alternate with more porous, finer laminae to generate a "pinstripe" texture. Compare with Fig. 12 for other examples of pinstripe textures. Part of image 1M141058680, acquired by the MI on sol 145 in complete shadow.

sediment transport in terrestrial eolian environments [26–28]. The systematic relationship between the apparent size of grains and the lamination of the bed supports the interpretation of the primary nature of these grains. In other cases, where primary grain boundaries are less evident due to the lack of differential

surface weathering, or because of secondary cementation or recrystallization (Fig. 7b–e), the presence of primary silt- or sand-sized sediment particles can be inferred due to the presence of cross bedding. In both eolian and subaqueous environments, the formation of cross-bedding requires transport of grains as a moving bedload layer at flow velocities which would suspend finer grains [29]. Thus, the presence of cross-bedding can be used as proxy for the presence of silt- and sand-sized grains.

Facies of the Burns formation include cross-bedded sandstone, planar-stratified to low-angle cross-stratified sandstone, wavy-bedded sandstone, and cross-laminated sandstone. In zones of intense recrystallization, massive deposits may also occur. However, even in these cases there generally is evidence of palimpsest layering, indicating that the primary deposits were not massive.

4.1. Cross-bedded sandstone

Cross-bedded sandstone is exposed in the Shoemaker's Patio locality of Eagle crater and at several places along the deeper rim of Endurance crater. It is well exposed at Burns Cliff, where it comprises the Burns lower unit. Bed sets range in thickness from 5 cm up to > 2.2 m. Internal stratification ranges from finely laminated (Figs. 8a), suggesting accretion through migration of wind ripples, to more thickly laminated, suggesting accretion through avalanching grain flows or through grain fall. The compound cross-bedding at Burns Cliff (Figs. 5b and 6a) shows evidence of both processes. Opportunity was not able to image any cross-bedding at Burns Cliff or other localities with the MI, and so grain size is undetermined. At Shoemaker's patio, cross-bed sets are interstratified with planar-laminated to low-angle cross-stratified facies. At Burns cliff, the large-scale cross-bed set is truncated and disconformably overlain by planar-laminated to low-angle cross-stratified facies.

The complex bedform geometry that is visible in the lower unit at Burns cliff (Fig. 5b) likely results from either the development of small-scale superimposed bedforms migrating over larger, primary bedforms to form "superimposition surfaces", or simple bedforms migrating under the influence of fluctuating airflow to create "reactivation surfaces" on the lee slope of an active bedform [30,31]. Reactivation surfaces are a common attribute of eolian cross-bedding and are thought to result, for example, from seasonal secondary oblique winds that episodically deflate dune lee slopes between intervals of dune advance that were controlled by the primary wind [32]. The distinction between superimposition surfaces and reactivation surfaces is subtle, but several criteria enable their assessment [30,31,33]. Reactivation surfaces tend to be cut at variable angles and generally are backfilled by cross-strata concordant with the surface. In contrast, superimposition surfaces are cut at low angles and almost always are backfilled with downlapping cross-strata. In the case of the Burns lower unit, the situation is made more problematic due to the oblique view angle of the outcrop as seen from the closest approach by Opportunity. Nevertheless, the weight of the evidence favors the development of reactivation surfaces associated with fluctuating wind conditions due to the variability of truncation angles and the largely surface-concordant geometry of backfill cross-strata.

The multimeter-scale cross-bedded sandstone facies is best interpreted to have been formed by migration of eolian sand dunes, for which a terrestrial analog is shown in Fig. 9a. Other possibilities include fluvial bar forms [34] or shallow marine, tidally generated bar forms [35]. However, tidal heights for Mars, dominated by solar tides, are estimated to be only 5–10% of terrestrial mean tides [36,37]. Thus, tidal currents on Mars high enough to generate meter-scale sand bars seem unlikely. Even if the resonant amplification effects due to embayed topography are considered, the probability still seems low because terrestrial meter-scale sand bars are associated with the highest known tidal-current velocities that develop in highly embayed topography [35]. Thus, since terrestrial multimeter-scale sand waves are associated with the highest tidal current velocities [35], the probability appears low that the Burns cross-bedded sandstone represents a tidal facies. The fluvial interpretation is also considered improbable, given associated facies—cross-beds at Shoemaker's patio are interstratified with planar-laminated sandstones, interpreted to have been formed by migration of wind ripples, and the large-scale cross-beds at Burns cliff are truncated and similarly overlain by planar-laminated, likely wind-ripple strata (see below). The few occurrences of this facies do not permit reconstruction of the specific eolian dune type. However, cross-stratification at Burns cliff is consistent with the presence of a single slip face, characterized by both grain flow and migrating ripples. This suggests the involvement of multiple wind directions in creating the dunes [38].

As a final point, it is worth noting that although this facies indicates transport of sand grains by wind-generated currents, the grains themselves were likely formed from an evaporitic source (see Discussion, and McLennan et al. [7]) and therefore water was involved in their formation.

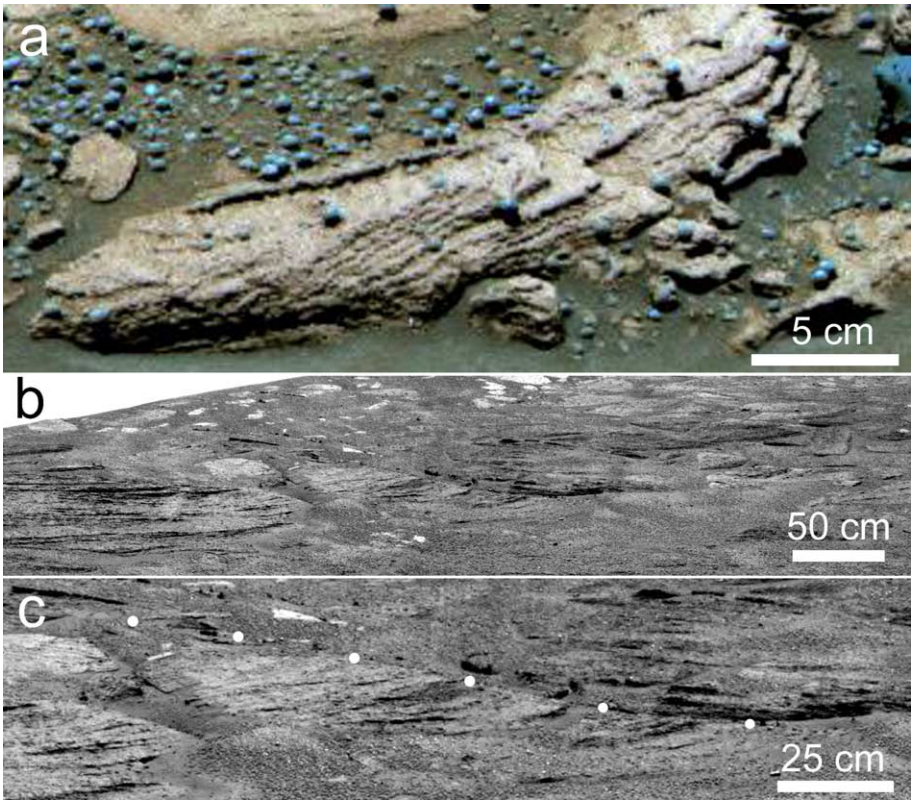

Fig. 8. Examples of cross-bedding as obtained by Pancam. (a) Thin (5 cm thick) bedset of tabular–planar cross-beds in breccia block ("Shoemaker's Patio", Eagle crater). Fine foreset lamination suggests accretion by migrating impact ripples across lee side of small eolian dune. Nearby breccia blocks are composed of fine-scale planar lamination and suggest that this bed occurs within the middle unit of the Burns formation. The image is a false-color composite generated from a subset of images acquired on Opportunity sol 50, sequence P2576, using Pancam's 750, 530, and 430 nm filters. (b) Laterally continuous truncation surface separates moderately dipping sets of cross-bedding within the lower unit of the Burns formation (west of Karatepe West, Endurance crater). The image was obtained by the Navcam, sequence P1920, on sol 169. (c) Enlargement of image shown in (b), showing details of cross-bedding. Note truncation of lower bedset and tangential downlap (to right in image) of overlying strata along truncation surface, highlighted by filled white circles. The massive, relatively thick cross-strata suggest accretion by grain flow, consistent with the observed downlap. The image was obtained by the Navcam, sequence P1920, on sol 169.

4.2. Planar-laminated to low-angle cross-stratified sandstone

Planar-laminated to low-angle cross-stratified sandstone is the most common facies of the Burns formation exposed in the four study areas of the Opportunity landing site (Figs. 10 and 11). At Burns Cliff it characterizes all of the Burns middle unit and much of the Burns upper unit, as is also the case for the Burns upper unit at Eagle crater. This facies is well-bedded, and is characterized by ubiquitous fine lamination except in zones of strong recrystallization (Fig. 12). For example, the upper 20–30 cm immediately beneath the middle–upper contact of the Burns formation is so severely recrystallized that primary stratification has mostly been erased (Figs. 6b and 11a).

The planar-laminated to low-angle cross-stratified facies typically shows fine lamination that is geometrically arranged in bed sets having horizontal to low-angle cross-stratification. Cross-stratification angles vary from 0° to 20° (Figs. 10 and 11). Other features include gently dipping, curved or irregular surfaces of erosion, small-scale cut-and-fill structures, convex-upward laminations, and occasional intercalation of high-angle eolian cross-bedding (Figs. 10 and 11). Where discontinuities occur, laminae can show angular disconformity with respect to the underlying surface.

The fine lamination itself is very likely the expression of alternating fine and somewhat coarser layers (Fig. 7a). The occurrence of mm-scale, parallel-sided lamination, expressed by changes in grain size, is consistent with the widespread development of translatent-ripple lamination. Translatent-ripple lamination [39] form as wind ripples migrate under conditions of bed accretion and each individual lamina is generated by the

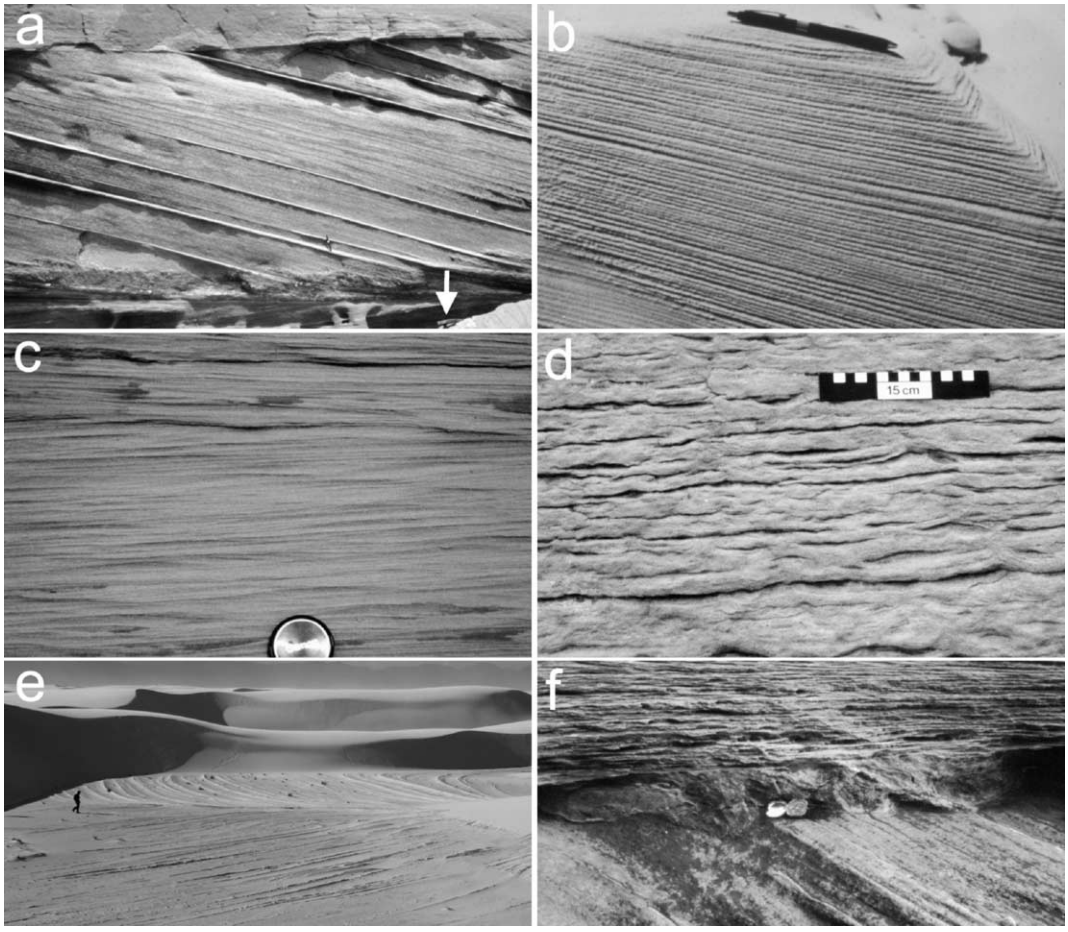

Fig. 9. Examples of ancient and modern terrestrial eolian stratification and truncation surfaces. All photographs, except (e), are courtesy of G. Kocurek. (a) Dune grain-flow cross-stratification, with thin ripple strata standing in relief, Page Sandstone (Middle Jurassic), Page, Arizona. Arrow points to hammer head, 18 cm in length. (b) Translatent stratification developed by migrating wind ripples, Recent, Padre Island, Texas. Pen is about 15 cm in length. (c) Translatent stratification developed by migrating wind ripples, Navajo Sandstone (Lower Jurassic), Red Rock State Park, Utah. Also note low-angle truncation surfaces. Scale is 55 mm lens cap. (d) Wavy to crinkly bedding, typical of what forms in a wet eolian environment, Page Sandstone (Middle Jurassic), Page, Arizona. In this case, the strata have accumulated above a regionally extensive deflation surface. (e) Holocene interdune deflation surface, White Sands, NM. Active, upwind dunes are visible in the background, whereas the foreground exposes the deflated foresets of the adjacent, downwind dune (from which the scene was photographed); wind-ripple laminae stand out in relief in contrast to grainflow/grainfall deposits, which are recessive. The deflated strata are weakly cemented due to the high solubility of the sulfate sand at White Sands. The depth of the scour and deflation is controlled by the elevation of the water table. This surface is interpreted as an analog for the Wellington erosional surface between the Burns lower and middle units (compare with Figs. 3, 4, 5a,b and 6a). Person for scale. (f) Ancient, water-table-controlled deflation surface, Page Sandstone (Middle Jurassic), Page, Arizona. This surface, which extends laterally for many tens of kilometers, is interpreted as a possible analog for the Wellington erosional surface between the Burns lower and middle units (compare with Figs. 3, 4, 5a,b and 6a). If the Wellington surface were as extensive as the Page surface, then it would suggest strongly that water table variations were regional in extent. Scale is opened geologic compass, 14 cm long.

translation of a single wind ripple (Fig. 9b,c). These ripples seldom have lee-side avalanche faces, but some grain size segregation results from coarser sand being concentrated close to the crestline. In this manner, the pinstripe texture characteristic of this facies could be developed (Fig. 12). Climbing of the ripples can be at angles either greater than (supercritical) or less than (subcritical) the slope of the stoss side of the ripples. Subcritical climbing of eolian ripples imparts well-defined, tabular lamination, usually a few millimeters thick, within which cross-lamination is not seen (Figs. 9b,c and 12). In contrast, supercritical wind-ripple lamination tends to produce wavy lamination and low-angle internal cross-lamination may be observed. The bulk of rocks seen in the Burns formation show clear evidence of tabular, mm-scale lamination and thus suggests subcritical climbing of eolian ripples as the cause of this stratification.

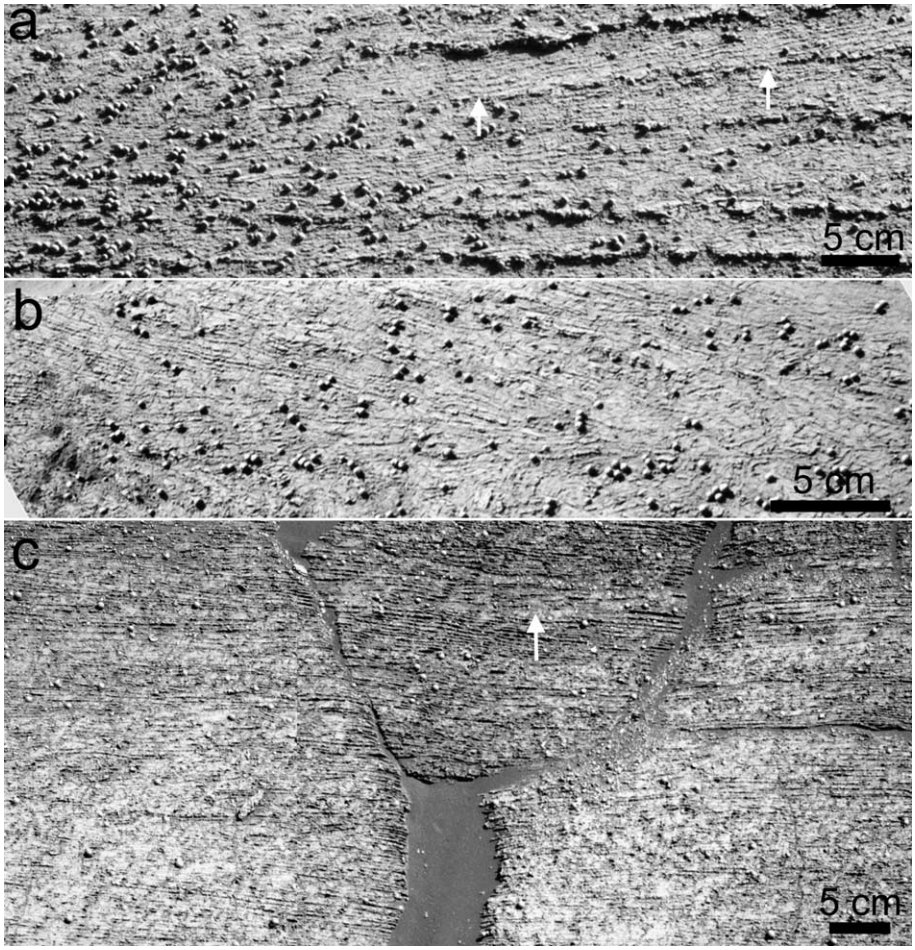

Fig. 10. Examples of planar-stratified to low-angle cross-stratified sandstone. (a) Finely laminated, climbing translatent strata ("Thales", rim of Endurance crater). Arrows indicate surface across which ripples formed and then began climbing from left to right. Translatent strata characteristically lack internal cross-stratification because eolian impact ripples lack steep slip faces. The image was obtained using Pancams 430 nm filter on sol 123. (b) Low-angle cross-stratification in breccia block ("Pyrrho") along rim of Endurance crater. The block is probably upside down as viewed by Opportunity, with stratal truncation being more evident from an inverted perspective. Nevertheless, the partial convergence of laminae from left to right suggests accretion within a low-relief bedform. The fine lamination indicates growth of the bedform by migration of subcritically climbing eolian impact ripples. The image was obtained using Pancam's 430 nm filter on sol 126. (c) Continuous interval of finely laminated, planar-stratified to low-angle cross-stratified sandstones in the middle unit of the Burns formation ("Karatepe West", Endurance crater). Note the numerous low-angle truncation surfaces. Also note the somewhat thicker lamination (arrow) that shows gentle climb to the right, consistent with climbing translatent cross-strata. The image is a grayscale composite generated from a subset of images acquired on Opportunity sol 312, sequence P2350, using Pancam's 430 nm filters.

The middle unit of the Burns formation is interpreted to represent the accumulation of an ancient sand sheet deposit, composed of sand grains derived from reworked evaporites (see Discussion, and McLennan et al. [7]) as in the base of the Burns lower unit. Low-angle eolian deposits of a sand sheet represent an important transitional facies between high-angle dune deposits (Burns lower unit) and associated interdune deposits (Burns upper unit). Occasionally, small dunes may have formed on the sand sheet, leading to intercalation and partial preservation of high-angle cross-stratification within otherwise planar-laminated facies (e.g. Shoemaker's patio: Fig. 8a). In many cases, such deposits signify the margins of ancient dune fields [40,41].

4.3. Wavy- and irregular-bedded sandstone

The wavy- and irregular-bedded sandstone facies occurs in the middle and upper units of the Burns formation. It includes a broad variety of features which likely record both primary sediment transport

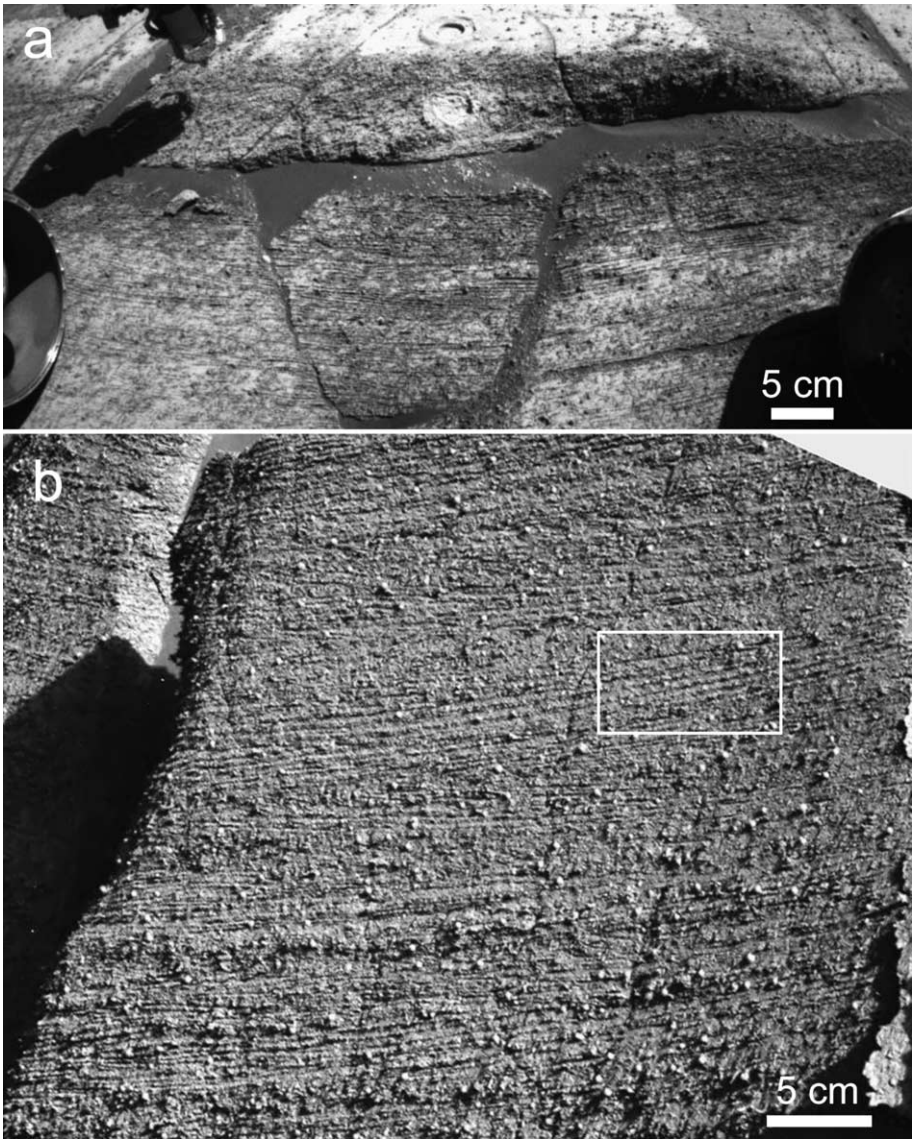

Fig. 11. Examples of planar-stratified to low-angle cross-stratified sandstone, cont. (a) View of Whatanga contact showing well-developed low angle stratification and truncation surfaces in lighter-toned, lower part of outcrop, beneath the contact ("Paikea-Wharenhui", Endurance crater). The image was obtained by the front Hazcams. (b) Spectacular example of low-angle cross-stratification featuring well-developed pinstripe texture which has likely formed due to differential cementation of translatent strata ("Tipuna", Endurance crater). The texture is particularly well developed in the left-dipping strata in the image center. The Tipuna outcrop represents the uppermost 30–40 cm of the Burns middle unit, and is just a few meters east of the outcrop shown in (a). White box shows outline of image enlargement shown in Fig. 12a. The image was obtained using Pancam's 430 nm filter on sol 307.

and post-depositional substrate modification. A wavy aspect may be imparted to the bedding due to shallow scours that are backfilled with laminae that trace the scour surface. These scours tend to be 5–10 cm wide and less than 1 cm deep (Fig. 13). These scour-and-fill structures may result from the erosive influence of one or more of several possible effects including local turbulence, changes in wind speed, changes in upwind topography, and fluctuations in surface wetness or sediment supply. An additional wavy appearance may be due, in some cases, to development of supercritically climbing wind ripples which preserve the primary ripple form. Trains of ripples could then create low-amplitude (few mm) wave forms. However, it is not possible to confirm this due to the lack of internal cross-stratification.

More irregular bedding is formed by distinct penecontemporaneous deformation features including con-

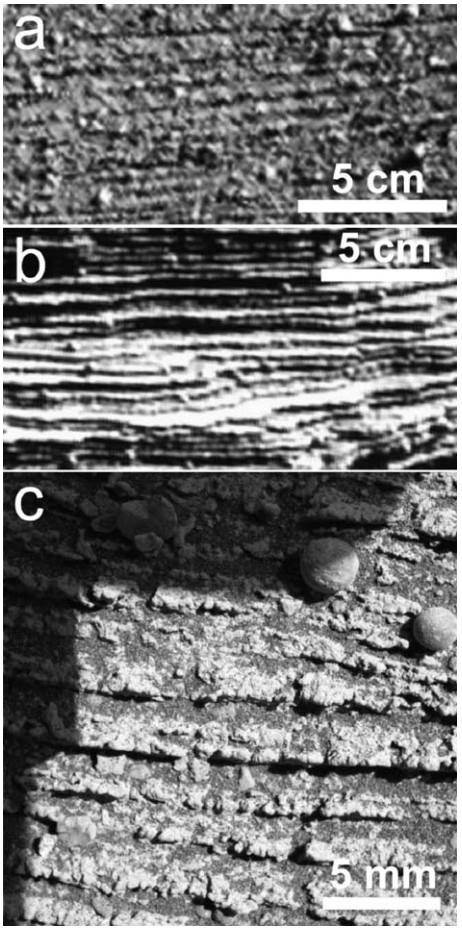

Fig. 12. Examples of "pinstripe" lamination texture. Pinstripe lamination is common in modern and ancient eolian sediments on Earth and is interpreted to record textural segregation of grain size, which leads to differential cementation within or adjacent to the finest sediments because of higher fluid capillarity [28]. In these examples, all pinstripe lamination appears to have been formed by migration of eolian impact ripples. In each example, note raised relief of regularly spaced laminae, suggesting a higher degree of lithification than adjacent laminae. (a) Enlargement of portion of image shown in Fig. 11b ("Tipuna", Endurance crater). The image was obtained using Pancam's 430 nm filter on sol 307. (b) Well-developed pinstripe lamination, with very even spacing of laminae (unnamed rock visible in Fig. 5c, Endurance crater). Grayscale "super-resolution image" using Pancam's 430 nm filter on sol 289. (c) Close-up of lamination detail confirming raised relief produced by surface etching of alternating, differentially cemented laminae. ("Wharenhui", Endurance crater). MI image 1M155707135, obtained on Sol 310 with illumination from upper right (shadow of instrument arm at upper left).

volute bedding, massive bedding with irregular vugs, and possible salt-ridge or small tepee structures (Fig. 13b–d). All of these features affect primary stratification dominated by fine, planar stratified to low-angle cross-stratified sediments of inferred eolian origin. The presence of discrete wind-laid layers with convolute bedding suggests that the water table may have been close to the surface. Evaporite minerals would have precipitated as interstitial minerals and cements, causing disruptive expansion and buckling of bedding to form irregular bedding. The salt-ridge or small tepee structures would have formed from concentration of salts at the air–sand interface because of evaporation of saline capillary water as inferred from studies of terrestrial analogs [42]. The accumulated surface salts cause expansion, forcing lightly cemented layers to rise and deform. Deformation may include both ductile (folds) and brittle (buckles) modes, depending on the extent of early cementation (compare Fig. 13b,d with Fig. 12c). In the Burns formation, brittle deformation features occur within laminae that show signs of potential early lithification, including lateral thickening of lamination and development of irregular laminae boundaries, and the formation of irregular vugs that could represent dissolved evaporite minerals. These irregular vugs differ from the more geometric vugs associated with inferred dissolution of euhedral diagenetic minerals [3,7], and could represent the precipitation of nodules of fine-grained, poikilitic evaporites due to capillary fluid rise, similar to what occurs in terrestrial sabkhas [43].

The wavy- to irregular-bedded facies is consistent with deposition in a dry to intermittently damp or wet interdune setting (Fig. 9d). The close association of planar to low-angle cross-stratified sandstones that have been modified by penecontemporaneous deformation and early diagenetic processes is diagnostic for this environmental interpretation [42,44]. In terrestrial analogs this facies most commonly accumulates as an interdune component and is often thin, forming intervals a few decimeters to a meter in thickness. However, these facies may form successions up to several meters thick, particularly above regionally extensive sequence boundaries where accumulation is driven by regional rise of the groundwater table (Fig. 9d).

4.4. Cross-laminated sandstone

Within the Burns formation that has been observed so far, the cross-laminated sandstone facies is least abundant. It is present within the upper part of the middle unit but is best developed within the upper unit (Figs. 14 and 15). The cross-laminated facies has been observed at both Eagle and Endurance craters and is best developed at Eagle crater owing to extensive impact-related brecciation at Endurance crater. Nevertheless, abundant blocks of this facies are observed within the Endurance breccia blanket (Fig. 15).

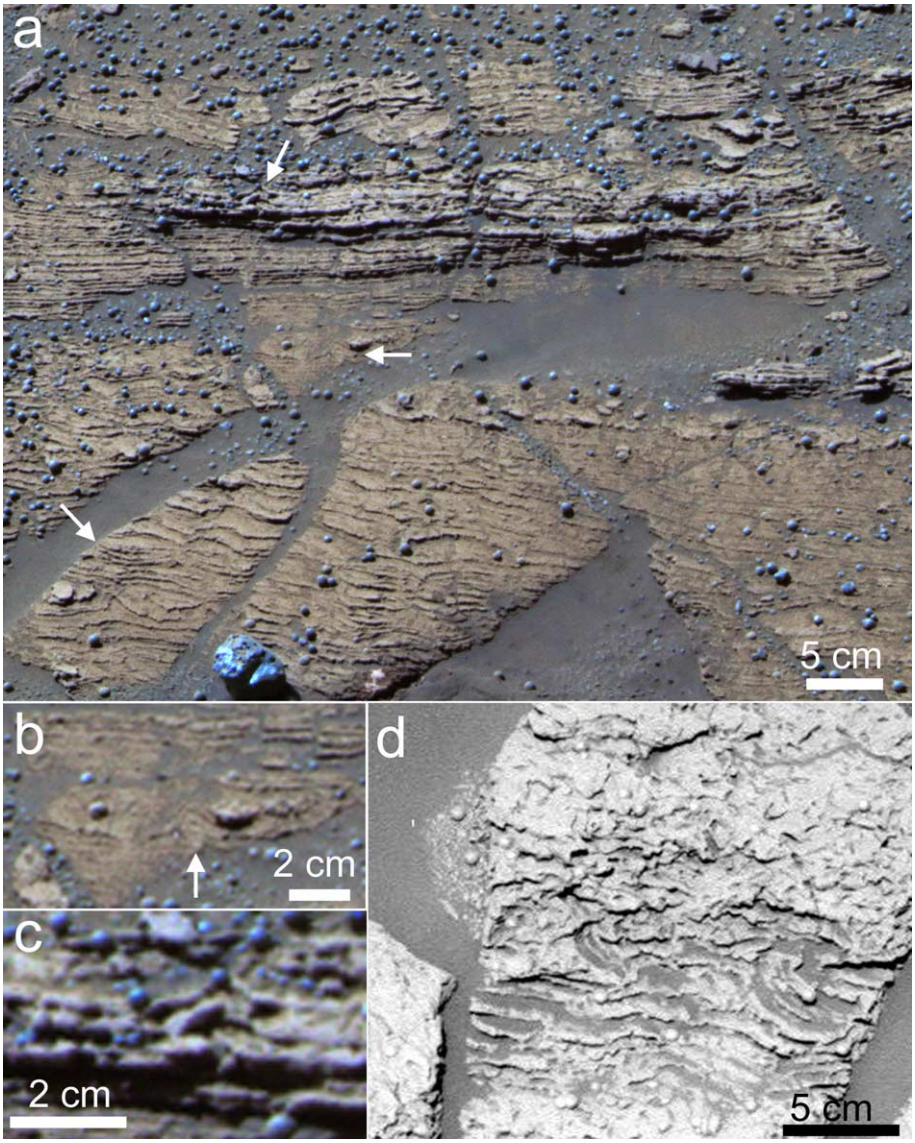

Fig. 13. (a) Various bedding textures interpreted to record damp interdune conditions ("Slickrock", Eagle Crater). Textures include fine-scale translatent lamination with pinstripe texture, irregular laminae with possible soft-sediment deformation features (upper, middle arrows), and wavy lamination associated with shallow scours (lower arrow). Wavy lamination also occurs at the top of the rock. The image is a false-color composite generated from a subset of images acquired on sol 045, sequence P2561, using Pancam's 600, 530, and 430 nm filters. (b) Close-up of feature at middle arrow in (a), showing soft-sediment fold structure. (c) Close-up of feature at upper arrow in (a), showing soft-sediment fold structure. Possibly broken fold hinge suggests that layering had been cemented early, to generate a small tepee structure. Alternatively it may be a "salt ridge" structure (see text for discussion). (d) Convolute bedding, overlain by massive, disrupted bedding consistent with damp to wet interdune conditions ("Big Bend", Eagle crater.). Note coherent bedding at base, which is progressively deformed upward to form small folds, and eventually incoherent bedding. The image was obtained using Pancam's 430 nm filter on sol 037.

4.4.1. Description

The cross-laminated sandstone facies can be recognized at a distance because of its distinct, differential weathering to produce a "ribbed" appearance (Figs. 14a and 15d,e), which is an order of magnitude more coarse than the "pinstripe" differential weathering which characterizes the planar-stratified to low-angle cross-stratified facies. An additional difference is the greater lateral discontinuity of bedding in the cross-laminated facies.

Sets of cross-laminae range from 0.3 to 1.8 cm in thickness (Figs. 14 and 15) and exhibit both tabular–planar and festoon bedset geometries. Bedsets generally show subcritical climb, but, a critical angle of climb may be present in the cross-laminae preserved in the

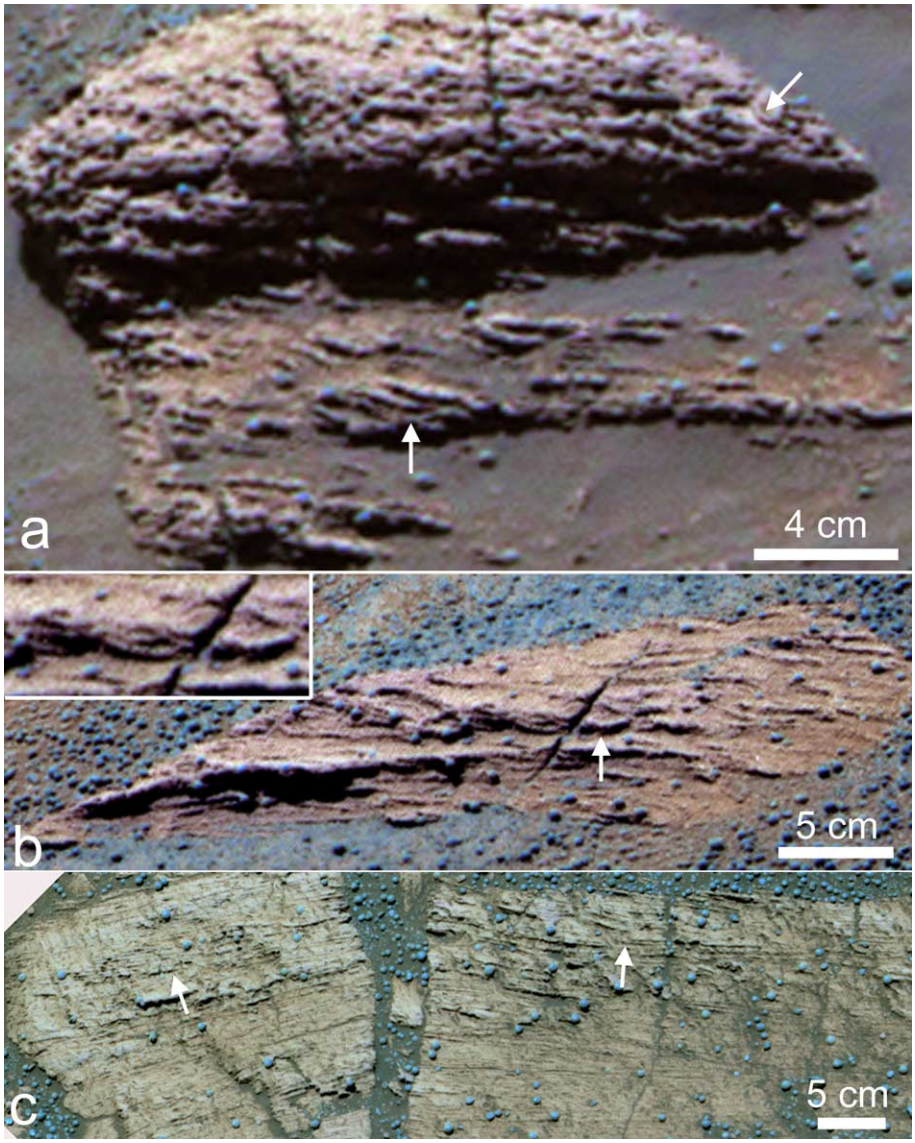

Fig. 14. Current-ripple cross-lamination. (a) Lower arrow points to set of probably planar cross-laminae, which suggest a small angle of climb from left to right. Note adjacent partial sets of cross-laminae which have similar geometry. Cut is likely parallel to flow, which was from left to right. Upper arrow points to example of cm-scale festoon cross-lamination ("Last Chance", Eagle crater). Small-scale festoon cross-stratification is indicative of 3D ripple geometry, which is known to develop only in subaqueous flows on Earth (see text). Note concave-up geometry of cross-laminae, upper bedset-bounding scour surface, and overlying cross-strata which downlap scour surface from left to right. Geometry of cross-laminae suggests that this is an oblique cut transverse to flow. The image is a false-color composite generated from a subset of images acquired on sol 017, sequence P2261, using Pancam's 750, 530, and 430 nm filters. (b) Cm-scale festoon ripple cross-lamination in breccia block ("Scoop") along rim of Eagle crater. Arrow points to set which has some suggestion of climbing from right to left. Inset shows detail, with potential climbing laminae straddling the crack in rock. Cut is obliquely transverse to flow, which would have had a small right-to-left component. The image is a false-color composite generated from a subset of images acquired on sol 052, sequence P2591, using Pancam's 750, 530, and 430 nm filters. (c) Broken blocks can be fit together to show complex assemblage of a several thin (few cm) sets of ripple cross-stratification, and fine, planar lamination with intersecting low-angle truncation surfaces ("Dells", Eagle crater). Cross-stratification at top (arrows) shows bedform migration to the right. The image is a false-color composite generated from a subset of images acquired on Opportunity sol 041, sequence P2544, using Pancam's 750, 530, and 430 nm filters.

lower part of Last Chance (Fig. 14a). Cross-laminae form bedsets that are up to 15–20 cm thick, such as at Last Chance. It is possible that bedsets were thicker because erosion and brecciation prevent tracing of the interval at Last Chance beyond the boundaries of the rock. However, the distribution of the "ribbed" weath-

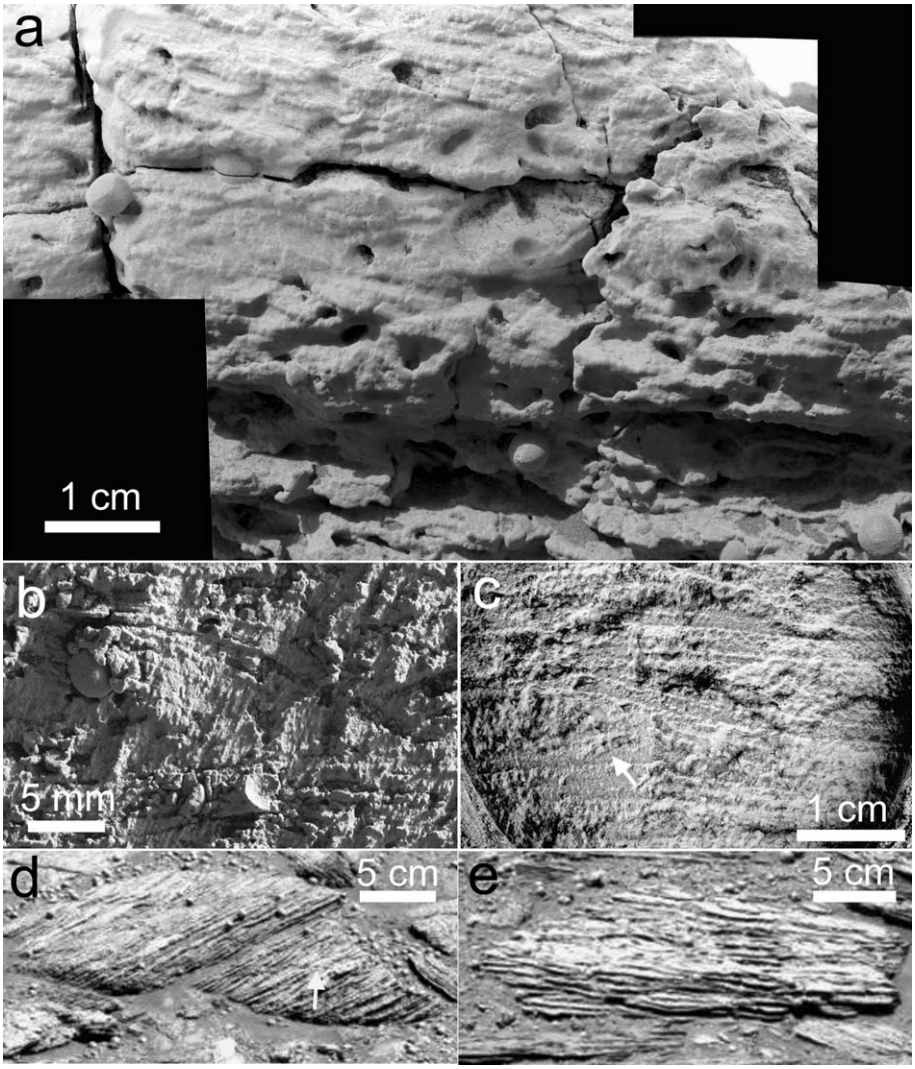

Fig. 15. Current-ripple cross-lamination, continued. The cross-lamination shown in "a" provides strong evidence for subaqueous sediment transport. The examples shown in "b–e" are consistent with subaqueous sediment transport, but are less conclusive than in "a". (a) An MI mosaic of several images showing the upper right part of "Last Chance" (Eagle crater), shown in Fig. 13a, shows festoon cross-lamination at variable, concave-up angles. The images in the mosaic were acquired by the MI on sol 058. (b) An MI mosaic of several images reveals a single set of ripple cross laminae suggesting a component of flow from left to right ("Kettlestone", Endurance crater). The images in the mosaic were acquired by the MI on sol 152. (c) An MI mosaic of several images obtained after use of the Rock Abrasion Tool reveals a rippleform with possible internal cross-lamination (see arrow) dipping to left ("Millstone", Endurance crater). Note onlap of rippleform by overlying laminae. The images in the mosaic were acquired by the MI on sol 162. (d) Arrow points to possible climbing ripple cross-lamination in unnamed rock along rover track at Karatepe West (Endurance crater). Angle of inferred climb is from right to left. The image was obtained using Pancam's 430 nm filter on sol 164. (e) Possible festoon cross-lamination in lower half of unnamed rock at Karatepe West (Endurance crater). Cut is approximately transverse to inferred flow direction. The image was obtained using Pancam's 430 nm filter on sol 136.

ering pattern in the Big Bend area (see Fig. 1 of Squyres et al. [3]) indicates that a minimum stratigraphic thickness for the cross-laminated facies could be on the order of 30–40 cm. It is possible that stratigraphically higher deposits of this facies are present in the uppermost part of the Burns upper unit, but the distribution of outcrop does not permit this observation at the landing site.

Ancient terrestrial cross-laminated deposits formed of sulfates are known from the Miocene of Spain [45]. Here, gypsum is precipitated within siliciclastic mudstones, so the resulting composition of the grains is a mixture of both silicate and sulfate minerals, similar to what appears to be present in the Burns formation of Meridiani [7]. These ancient deposits have been subjected to aqueous diagenesis and are

locally recrystallized, resulting in partial obliteration of primary textures, similar to what is observed in the Burns formation.

4.4.2. Bedform reconstruction

The ripple cross-lamination observed in the Burns formation is consistent with two-dimensional to three-dimensional bedforms, climbing at generally stoss-erosional, lee-depositional, positive angles [46]. Two-dimensional bedforms are suggested by the cross-lamination present in the lower part of Last Chance (see lower arrow in Fig. 14a). These would have had straight crestlines, and constant-elevation crestlines and troughs. However, it is also possible that this is a flow-parallel cut through a set of cross-strata that might be festoon-shaped in the orthogonal cut, and therefore indicative of a three-dimensional bedform. The exposure is not good enough to make this distinction.

Festoon cross-lamination is present in the upper part of Last Chance (see upper arrow in Fig. 14a) and in Scoop (see arrow and inset box in Fig. 15), which is diagnostic for three-dimensional bedforms. In contrast to two-dimensional bedforms, these three-dimensional bedforms would have had either sinuous crestlines or sinuous troughs, either in planform or in elevation, or both [46]. Fig. 16a shows the results of a computer simulation of propagating bedforms which could generate cross-lamination with both festoon geometry (as viewed normal to flow direction) and tabular–planar geometry (as viewed parallel to flow direction). Bounding surfaces scoured by three-dimensional bedforms tend to be trough shaped, in contrast to the planar bounding surfaces generated by two-dimensional bedforms [46]. A terrestrial analog for this sort of festoon cross-lamination is shown in Fig. 16b. The rock exposes two faces at nearly orthogonal intersection and illustrates well the possibilities for the interpretation of the Burns formation cross-lamination.

The presence of positive climb angles in some examples indicates sediment deposition during bedform migration [47]. These conditions could be met in a flow which undergoes a downcurrent decrease in transport rate where the near-bed velocity decreases. In this situation, sediment can be transported to the site of deposition while bedform migration rates are slowing. Such a structure is predicted to occur most commonly in shallow fluvial flows, where deposition from suspension would be very rapid [27].

Ripple bedforms of the type observed in the Burns formation have been well studied in laboratory and natural systems on Earth [29,48–51], as well as theoretically for both Earth [46] and Mars [52]. The festoon

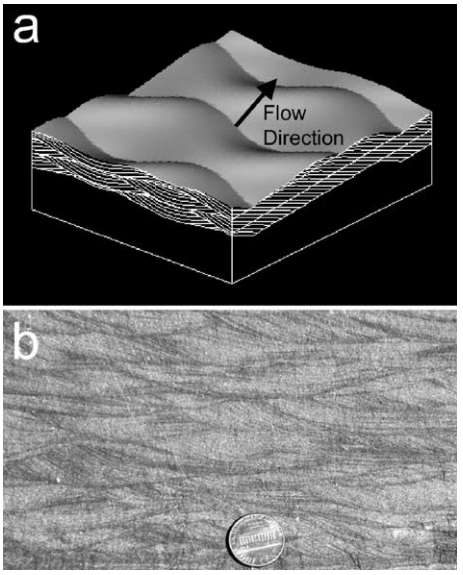

Fig. 16. (a) Computer simulation of 3D ripple bedforms that are transverse to flow, with curved, out-of-phase crestlines. Cross-lamination sets with festoon geometry are produced by bedforms that have closed topographic depressions (scour pits) in their troughs. Migration of the leading (erosional) side of the depression scours a trough-shaped bounding surface, and migration of the trailing side of the depression results in deposition of the cross-laminae. After Rubin [46], Fig. 34. (b) Outcrop photograph of cm-scale festoon cross-lamination in 1.4 Ga Mt. Shields Formation, Belt Supergroup, Montana. The flows responsible for cross-lamination of this type are regarded to have formed in very broad, shallow channels (perhaps only a few decimeters deep) near the lower reaches of regionally extensive alluvial fans which developed across unvegetated landscapes of the early Earth [98].

cross-lamination observed in the Burns formation, implying highly sinuous bedform crestlines, is known to develop only in subaqueous ripples. In contrast, eolian impact ripples have very straight crestlines and their migration generally does not produce festoon cross-lamination. Indeed, the tabular–planar cross-lamination which is produced is often not well expressed and is inclined at angles much lower than the angle of repose [33,39,53]. Instead, the "pinstripe" lamination defined by inversely graded mm-thick layers is often the diagnostic attribute of eolian wind-ripple migration [28,39]. On Earth, it is possible for small-scale eolian dunes to develop more sinuous crestlines, but their lower size limit seems to be on the order of 10 cm. Furthermore, these bedforms are not sinuous enough to produce the cm-scale festoon cross-lamination observed in the Burns formation. These small dunes typically have sinuosities with wavelengths on the order of decimeters or more [54] rather than centimeters, which would be required to produce Burns festoon cross-lamination. However, we cannot rule out the possibility that

under rare circumstances smaller wavelengths might occur; if so, we are not aware of a specific example.

Experiments on eolian sediment transport suggest that unusually sinuous ripple-like bedforms can form under very particular circumstances (see Fig. 5.5 in Greeley and Iverson [55]). Unfortunately, these experimentally generated bedforms were not dissected to ascertain stratification geometry. Additionally, these experiments were done with 30-μm-size glass spheres, which is significantly finer than the grain size (300–800 μm) measured for the Burns formation, and the grain density of Burns sediment particles may have been significantly different being composed of an admixture of silicate and sulfate minerals [7,8]. It seems likely that the density ratio ($\rho_{\text{sediment}}/\rho_{\text{fluid}}$) of this experiment is very different from that of Mars, given the very significant difference in atmospheric density. Regardless of this experimental result, observations of recent eolian processes on Mars appear to limit the role of wind in accounting for the festoon cross-lamination present in the Burns formation. At the time of this writing, the combined travel distance for both the Spirit and Opportunity rovers now exceeds 10 km, yet no evidence has been seen for morphologies which could produce cm-scale festoon cross-lamination, despite abundant evidence for eolian bedform development [56,57]. Wind ripples observed by Opportunity on the plains and in the craters of Meridiani occur as two types: fine grained, with low amplitudes of much less than one cm, or coarse-grained (>1 mm) and with amplitudes of 1 cm or more [57]. In both cases the crest lines are very straight and these bedforms show no evidence of being able to form festoon cross-stratification during migration. Trenching revealed a homogenous internal structure in the case of the coarse-grained ripples. Small dunes with potential slip faces also were observed by Opportunity in the floor of Endurance crater. These bedforms resemble terrestrial star dunes and have long arms that extend away from the core of the dune complex, which suggest multiple wind directions in their formation. These arms have especially straight crests and, again, present an unsuitable geometry to create the cm-scale festoon cross-lamination present in the Burns formation. Other observations of eolian bedforms on Mars at the Pathfinder or Viking sites [58,59] similarly lack evidence for morphologies which could produce cm-scale festoon cross-lamination.

4.4.3. Hydrodynamic considerations

All aspects of flow and sediment transport by steady uniform flows of a Newtonian fluid like water in open channels can be described by a discrete set of variables. There are several different sets which can be defined, but the following set is particularly useful in this context: mean flow velocity U, mean flow depth d, sediment size D, fluid density ρ, fluid viscosity μ, grain density ρ_s, and submerged weight per unit volume of the sediment γ' [29]:

$$\text{Bed configuration} = f(U, d, D, \rho, \mu, \rho_s, \gamma'). \quad (1)$$

The variables in Eq. (1) can be used to describe bed configurations, including the development of the three-dimensional ripples inferred to have produced the festoon cross-lamination in the Burns formation. Note that the influence of the acceleration of gravity is specified in γ', which will be discussed further below as it relates to changes in the physical interpretation of open-channel flow on Mars as compared to Earth. By dimensional analysis, the variables in Eq. (1) can be grouped into dimensionless variables that characterize the flow [29,60]. The sedimentologically most interesting set separates d, U, and D:

$$\begin{array}{l} \text{Dimensionless flow velocity } U^\circ = U(\rho^2/\mu\gamma')^{1/3} \\ \text{Dimensionless flow depth } d^\circ = d(\rho\gamma'/\mu^2)^{1/3} \\ \text{Dimensional grain size } D^\circ = D(\rho\gamma'/\mu^2)^{1/3} \\ \text{Density ratio } \rho_s/\rho \end{array} . \quad (2)$$

This set of dimensionless variables provides a complete set of scale-modeling parameters that can take into account a wide range of sedimentologically interesting behaviors such as the effects of changing grain size, current velocity, flow depth, fluid viscosity (via temperature change), grain density, and the acceleration of gravity. Although all these effects can logically vary for different situations on Earth or Mars, or between Earth and Mars, only the last of these effects is *required* to change for flows on Mars versus Earth. Fortunately, the change in the acceleration of gravity is known; other variables are imprecisely known, or worse yet, unknown. Therefore, it is important that we consider here what can be determined and what must be assumed. The good news is that in several cases the influence of these unknowns is small.

For the purpose of this analysis, we will assume reasonable values for the unknowns. This includes fluid viscosity and density (assume water at 10 °C), grain density (assume quartz), and flow depth (likely to have been shallow). We know a priori that g is contained in γ', and that $g_M \approx 0.4 g_E$ (where g_M and g_E are the values of the acceleration of gravity on Mars

and on the Earth, respectively). Therefore, the actual values of d, U, and D would be different in two dynamically similar flows on Mars and Earth even if the water viscosity (mostly affected by temperature) were the same [52]. Scale factors which relate the sense and magnitude of the effects of Mars' different gravitational constant are considered later.

The initiation of sediment motion and the bedforms which develop as a result of grain–fluid interactions can be displayed on multi-dimensional graphs which show the stability of the various bedforms based on observational data [29,61]. The observational data–collected during careful experiments–are then plotted so that the various bedforms occupy contiguous stability fields, with boundary surfaces separating the fields [61]. A three-dimensional graph of flow depth, bed shear stress, and grain size is most commonly used to illustrate the effects of these most important parameters. However, the effects of flow depth may be neglected if only shallow flows are considered, which is appropriate for the inferred interdune depositional environment of the Burns formation upper unit. Furthermore, since the velocity of most natural flows is the most important component of bed shear stress then we can accept flow velocity as a surrogate for bed shear stress. Thus, the simplest representation of the system is provided by a two-dimensional graph (Fig. 17a), which relates the bed configuration to flow velocity and grain size, normal-

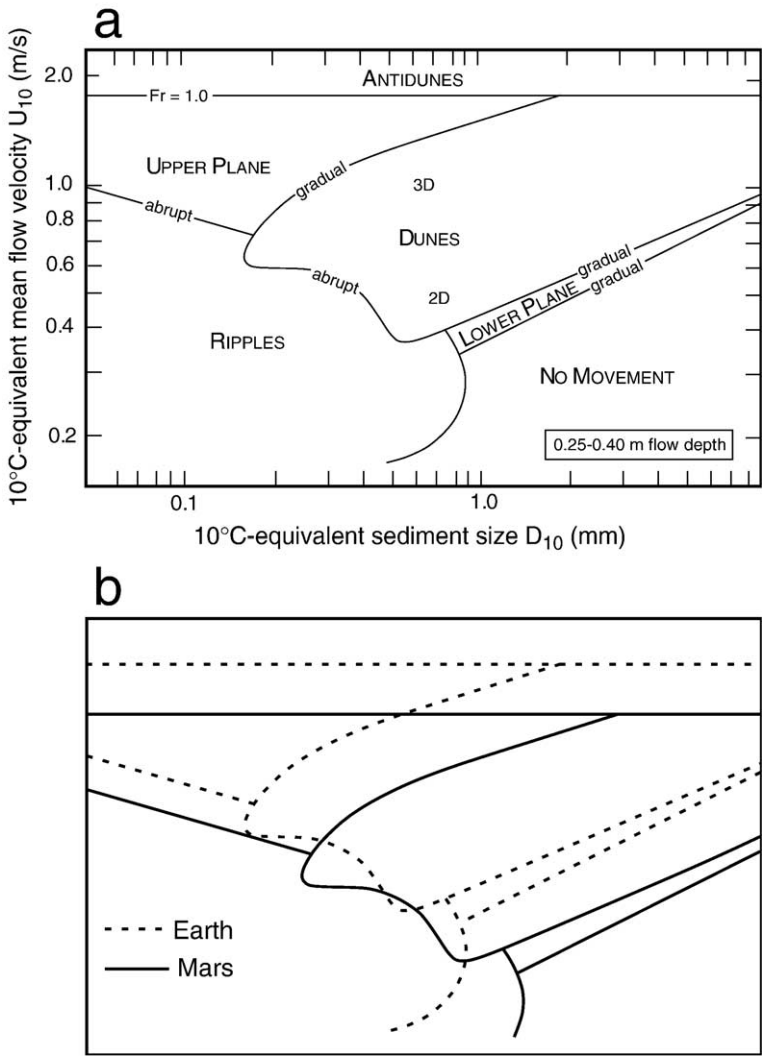

Fig. 17. (a) Dimensionless velocity–size graph for 10 °C-equivalent flow depths of 0.25–0.40 m. Upper Plane and Lower Plane refer to bed configurations where neither ripples nor dunes exist. Antidunes occur at mean-flow Froude numbers somewhat smaller than 1.0. After Southard and Boguchwal [60]. (b) Rescaling of dimensionless velocity and grain size for effect of reduced acceleration of gravity on Mars.

ized to 10 °C water temperature and flow depth of 0.25–0.40 m [60].

This velocity–size graph provides some guidance to the likely range of flow velocities, given a particular bed configuration and grain size. Since we have reconstructed the bed to have consisted of three-dimensional ripples we need only obtain an estimate of grain size. The lower range is difficult to obtain because of diagenetic effects associated with recrystallization, and because the lower limit of resolution of the MI is 30 μm/pixel, which means that the smallest resolvable grains would have a diameter of about 0.1 mm. However, as Fig. 17a illustrates, it is the upper limit which is more important because above a certain limit ripples do not develop. Our measurements of grain size in the Burns formation indicate that most sediment has a grain size finer than 0.3–0.8 mm, and the coarsest particles observed are up to 1.0 mm. This upper limit is close to the no-ripple boundary, but, the finer-grained particles could have formed ripples. Indeed, the evidence for three-dimensional ripples having actually formed in the Burns formation is not violated by any of these terrestrial experimental data. Assuming a lower grain size of silt, this generates a range of possible flow velocities of 0.1 to 1.0 m/s for the currents which formed the three-dimensional ripples of the Burns formation. If larger grains were involved, then the maximum velocities would have been a bit slower.

The estimates for flow velocity obtained above are subject to adjustment as a result of the different acceleration of gravity for Mars. Southard and Boguchwal [52] have considered how this difference may influence resulting bed configurations, assuming cohesionless quartz-density sediment. (This assumption is clearly incorrect for the Burns formation, but its effect on the density ratio ρ_s/ρ may be small; the density of quartz is 2.65 g/cm^3 and the densities of the likely mixture of sulfate evaporite minerals thought to partially compose the Burns formation range from 1.9 to 3.2 g/cm^3, so perhaps the mean density of the Burns mineral assemblage in water is not significantly different from the density of quartz in water.) Eq. (2) shows that each axis of the dimensionless velocity-size graph contains g via γ', but because $g_M \approx 0.4 g_E$ the actual values of U and D would be different in two dynamically similar flows on Mars and Earth if the water temperature was the same. To provide an idea of these effects Southard and Boguchwal [52] computed the scale factors by which the axes of the velocity-size graph standardized for some temperature on Mars are multiplied relative to the velocity-size graph standardized for the same temperature on Earth. To obtained the scale factors solve for the ratios U_M/U_E and D_M/D_E:

$$U_M\left(\frac{\rho^2}{\mu\gamma'_M}\right)^{1/3} = U_E\left(\frac{\rho^2}{\mu\gamma'_E}\right)^{1/3};$$
$$\frac{U_M}{U_E} = \left(\frac{\gamma'_M}{\gamma'_E}\right)^{1/3} = \left(\frac{g_M}{g_E}\right)^{1/3} = 0.74$$

$$D_M\left(\frac{\rho\gamma'_M}{\mu}\right)^{1/3} = D_E\left(\frac{\rho\gamma'_E}{\mu}\right)^{1/3};$$
$$\frac{D_M}{D_E} = \left(\frac{\gamma'_E}{\gamma'_M}\right)^{1/3} = \left(\frac{g_E}{g_M}\right)^{1/3} = 1.36 \quad (3)$$

where U_E, D_E, and γ'_E are the velocity, grain size, and submerged weight per unit volume of the sediment in the terrestrial flow and U_M, D_M, and γ'_M are the respective variables in the Martian flow.

The first set of equations indicate that a given transition between bedforms, say ripples to upper plane bed, at constant grain size and flow depth, occurs at a lower velocity on Mars as compared to Earth, by a factor of 0.74. The second set of equations indicate that a similar transition between bedforms, at constant velocity and flow depth, occurs at a larger grain size on Mars as compared to Earth, by a factor of 1.36. This small, but non-negligible effect is shown in Fig. 17b. The important point is that ripples should be easily formed in shallow subaqueous flows on the surface of Mars given the observed range of grain size. The change in g, as well as potential changes in grain density or even water temperatures [52], pose little challenge to this prediction.

4.4.4. Summary of the case for sediment deposition by flowing water

The case for flowing surface water is based on the following observations and supporting constraints:

1) The images in Figs. 14a,b and 15a show evidence for festoon cross-lamination. The bedform morphology required to produce such cross-lamination is characteristic of ripples with highly sinuous crestlines, with wavelengths on the order of a few cm.
2) On Earth, these bedforms form only in water. The possibility that such bedforms developed under natural conditions by other processes is remote. Dimensional analysis shows that sediment transport and development of bedforms on Mars is not likely to differ substantially from Earth.

3) In the combined travels of both Opportunity and Spirit, along with observations from earlier landed missions to the surface of Mars, no eolian bedforms have been observed which could explain the festoon cross-lamination observed in the upper part of the Burns formation.

5. Facies associations and depositional environments

The term *facies association* denotes a group of facies that are genetically related to one another and that have similar environmental significance. The facies of the Burns formation combine to form three distinct facies associations, which represent sediment accumulation under varying physical processes which characterize a dune–interdune system. All are formed by accumulation of sand grains derived from evaporites with a significant siliciclastic component (see Discussion, and McLennan et al. [7]). These facies associations are eolian dune, eolian sand sheet, and damp to wet interdune. The available data do not allow us to determine the lateral scale of these depositional elements, but it seems likely that the interdune depression extended at least the 1 km distance from Eagle crater to Endurance crater.

5.1. Eolian dune

The eolian dune facies association is formed exclusively by the cross-bedded sandstone facies, which forms the entire Burns formation lower unit (Fig. 3). As described above, these large-scale cross-beds are indicative of sediment transport within large dunes (>2 m) that had modified slip faces resulting from reactivation or the superimposition of smaller bedforms. The presence of eolian dunes on the ancient surface of Mars is not unexpected and suggests an at least episodically dry climate within the region. It is not possible to constrain the lateral extent of this paleodune field; however, regional considerations suggest that it may have been widespread due to the significant lateral continuity of the Burns formation as inferred from TES and MOC data.

5.2. Eolian sand sheet

Sand sheet deposits are the dominant facies association in the Burns formation middle unit (Figs. 3 and 4). The association is composed mostly of planar-laminated sandstone and low-angle cross-stratified sandstone, with intercalated but relatively uncommon intervals of cross-bedded sandstone and rare cross-laminated sandstone.

Sand sheet deposits may form a transitional facies between dune and interdune deposits and fluvial deposits, and represent the accretion of wind-blown sand under conditions that are not favorable to dune development [41,62]. Several factors contribute to terrestrial sand sheet formation, including: (1) a high water table, (2) early cementation, (3) wetting during episodic floods, and (4) significantly coarse-grained sediment [41]. All of these potential effects are plausible in the case of the Burns formation. Rather than forming dunes, these factors result in development of broad, low-relief undulatory surfaces which extend across a sandy plain.

The dominant depositional process in sand sheet settings is ripple-related, including granule ripples (very coarse-crested ripples; [53]). Even if granule-caliber sediment has not been introduced into the system, these deposits will tend to accumulate coarse grains. In the Burns formation, this may be limited to grains up to 1 mm; coarser grains have not yet been observed. Sand sheet deposits as recognized in eolianites commonly consist of nearly horizontally stratified detritus. Such deposits are commonly sandstones that are finely laminated and contain only low-angle discordances, developed during the migration of low-relief mounds of sand. Advance of these morphologic elements, which commonly dip downwind, never occurs by slip-face processes such as grain flow, but rather by saltation and accretion of wind-ripple translatent strata [41,62]. Uncommonly, small dunes with active slip faces may form in sand sheets, and rare flood events may cause fluvial reworking of eolian sediments. It is likely that the middle unit of the Burns formation records both of these uncommon events, through the preservation of cross-bedding (Fig. 8a) and ripple cross-lamination (Fig. 15b,c).

5.3. Interdune

The physical facies attributes and stratigraphic architecture of the Burns formation upper unit compare well with eolian interdune systems on Earth. In these well-studied terrestrial analogs, the relationship between geomorphic components (dune, sand sheet, interdune) is strongly controlled by oscillations of the water table and changes in sediment flux [42,63]. Geomorphically, an interdune depression is a surface commonly enclosed or at least partially bounded by dunes or other eolian deposits such as sand sheets [42]. Interdune depressions may be as small as the trough between individual dunes or as large as playa lakes ranging up to several kilometers or tens of kilometers in diameter.

In addition, we note that the facies assemblages in the Burns middle and upper units might also be consistent with accumulation above a regionally extensive sequence boundary that truncates an entire dune–interdune system (cf. [63–65].

The sedimentology of interdune facies associations is complex and strongly dependent on climate and elevation of water table [44]. These factors influence the sedimentology of interdune deposits, and also help determine if the interdune is deflationary or depositional. Where depositional, interdune facies associations are classified as "dry", "damp", "wet", or "evaporitic" depending on the relative abundance of sedimentologic indicators of liquid–water-induced processes and to what extent minerals are precipitated if the water evaporates [42,44,66]. There is no sharp distinction between these associations due to the highly ephemeral involvement of water as it moves up and down across the sediment–water interface and through the shallow subsurface. Interdune facies are characterized by sedimentary structures ranging from subaqueous current and wave ripples, wavy laminae (wet depositional interface), adhesion structures, desiccation cracks, and wind-ripple stratification (damp to dry depositional interface) [42,44,67]. In the case of wet interdune deposits, the water table is shallow and the depositional surface is within the capillary fringe of the water table. Wet interdune environments developed in semiarid to arid climates will also tend to accumulate evaporite salts. In this case, the interdune will form a playa; the larger the interdune, the larger the playa. The Whatanga contact, which separates the middle and upper Burns units, is interpreted as a diagenetic front associated with a stagnant water table. A zone 30–40 cm thick beneath the Whatanga contact shows significant evidence for recrystallization (Figs. 5c and 6b) of finely laminated sandstones beneath the contact itself but without an associated change in primary facies.

The occurrence of subaqueous current ripple cross-lamination and wavy to irregular-bedding in the upper unit of the Burns formation is consistent with sediment accumulation in a damp to wet, evaporitic interdune environment. The occurrence of convolute bedding, along with possible "salt-ridge" or small tepee structures supports this interpretation [42,68]. These penecontemporaneous deformation features are developed in situations where the water table is close enough to the surface so that the capillary fringe influences both sediment cohesion and the precipitation of minerals and volume changes related to thermal and early diagenetic effects. The formation of current-ripple cross-stratification requires intermittent surface flow of water characterized by unidirectional currents associated with flooding of interdune depressions.

6. Discussion

6.1. Significance of stratigraphic bounding surfaces

The problem of how bedding and bedding planes originate is a fundamental challenge for stratigraphers. Quantitative analysis of terrestrial sedimentary strata shows that partitioning of rock volumes between stratigraphic surfaces is strongly dependent on the interaction of base-level change, sediment flux, and the time scale over which sediment accumulation is considered [12,69–71]. This point is supported by a century of field investigations [72–76] which show that in constraining the dynamics of sediment accumulation a proper understanding of stratigraphic omission surfaces is as important as understanding rock volumes and facies. In the context of inter-regional eolian systems, base level is strongly influenced by the water table, which controls how much sediment enters the rock record and how disconformities are distributed [63,66,77,78].

The contact ("Wellington") which separates the lower and middle units of the Burns formation may provide significant insight into the past role of groundwater in controlling the stratigraphy of the Burns formation (compare Figs. 4, 5a,b, 6a with Fig. 9e,f). Irregular, scoured surfaces of this type are the distinctive signature of wind erosion of moist or lightly cemented, cross-bedded eolian sand [79]. By analogy with terrestrial eolian systems, this erosional contact can be interpreted as an interdune deflation surface, created by a rise in the water table to partially preserve eolian dune strata [77,78]. Local shallowing of the water table to the depositional surface or within its capillary fringe would have increased moisture–and therefore the erosional threshold–to the point where the interdune surface became increasingly protected from erosion (Fig. 9e,f). A water table forms a downward limit of scour through the cohesion of damp or wet sand, and through early cementation by evaporite minerals precipitated in the sediments as water evaporates near the air–sand interface [80]. On Earth, these surfaces develop in association with changes in the water table in excess of 10^2 yrs and can be basin-wide–representing deflation requiring removal of entire sand seas, or local–requiring only local reorganization of the dune field [63,78].

A more regional interpretation for the Wellington erosional surface also is possible. Lateral mapping of erosion surfaces in terrestrial eolian systems shows that

truncation can be related to regional–in this case at the scale of the Meridiani sediment basin itself–oscillations in the water table [63–65]. In this hierarchal approach to surface classification, these "supersurfaces" would truncate strata related to lateral migration (and climb) of a dune–interdune system. Thus, true interdune surfaces are more limited in scale, with supersurfaces acting to partition the rock volumes at a regional scale. However, our data do not permit us to distinguish between interdune surfaces and supersurfaces because of the limited lateral extent that we can trace the Wellington contact. Regardless of which interpretation is correct–true interdune deflation surface versus regionally extensive truncation surface–each is consistent with an increase in sediment moisture content above the Wellington contact.

The presence of eolian rather than fluvial deposits immediately above the Wellington contact suggests that the erosional surface here became damp but was not flooded. In cases where rapid flooding of dunefields has been documented on Earth [81–83] substantial preservation of fragile dune topography occurs rather than abrupt truncation. In addition, significant slumping of dune foreset strata is observed. Although the exposed length of the Wellington contact is just a few meters, neither of these features is observed, suggesting that the truncated crossbeds of the Burns lower unit were damp or partially cemented prior to truncation. Consequently, a model involving slow rise of the water table through an active dune field, followed by eolian deflation, is invoked as the truncation mechanism.

This is important for interpreting the processes by which liquid water was made available on the early surface of Mars. Though there is ample evidence for rapid venting of water to form incised topography [9] and even meandering river deposits [2], the Wellington contact provides clear evidence for ordinary oscillation of the groundwater table, which may not have become fully emergent at this location until the accumulation of the Burns upper unit. However, surface water supplied by rapid venting could have infiltrated highlands adjacent to the Meridiani basin to recharge the basin groundwater system, which then might have relaxed over longer time scales. The important conclusion is that the stratigraphic architecture of the Burns formation is more consistent with slow discharge of groundwater than it is with vigorous overland flow.

6.2. Significance of sulfate eolianites

Geochemical and mineralogic data show that the Burns formation studied so far is composed entirely of "dirty" evaporites [3–6,8] formed of a mixture of fine clay or silicate minerals embedded in "sand" grains of sulfate and possibly chloride salts. Sedimentologic and stratigraphic analysis of the same rocks, however, indicates that only a small percentage of rocks were formed by transport of grains in water. The rest are interpreted here to have formed by transport of evaporite grains in wind to form a variety of eolian facies. However, because these grains are made of evaporites this requires an evaporite source area, and therefore water, to have been temporally equivalent to (or older than) these eolian deposits.

Confirmation of the evaporitic composition of Burns eolian facies is provided by mini-TES data from the large-scale cross-bedding of the Burns formation lower unit, exposed at the eastern end of Burns cliff. These data suggest no significant difference in composition between the large-scale cross-bedded facies (Fig. 18, "Lower Wellington") and the overlying planar-laminated to low-angle cross-stratified facies (Fig. 18, "Upper Wellington"). In addition, there is no significant difference as compared to Burns outcrops thought to have been deposited in water (Fig. 18, compare "Wellington" measurements with "Last Chance" measurements). These observations constrain the composition of the eolian sediment particles that built these ancient dunes to be composed of a significant fraction of evaporite, nearly identical to that of stratigraphically superjacent facies.

Mineralogic and geochemical observations of the Burns middle unit [8] show that eolian sand sheet facies also are significantly evaporitic. The mini-TES data shown in Fig. 18 ("Upper Wellington" observation) indicate that sand sheet deposits at the base of the Burns middle unit have a significant sulfate component. In addition, APXS and Mossbauer data [8] indicate that finely laminated sand sheet facies of the upper part (e.g. "Millstone", "Manitoba") of the Burns middle unit also are composed of a significant fraction of sulfate minerals. Though these sediments formed sheets instead of dunes, we still interpret their source to have been a nearby playa undergoing deflation to provide a flux of evaporite grains to a downwind site of deposition.

The significance of these observations is to indicate that liquid water was involved in the production of eolian sand particles. This requires an evaporite basin (interdune depression or playa lake) to have been spatially adjacent and therefore *temporally equivalent* to the dune field and sand sheet represented by the Burns formation lower and middle units. This evaporite basin would have been reworked by the wind to supply a flux of grains that were then blown into duneforms. A

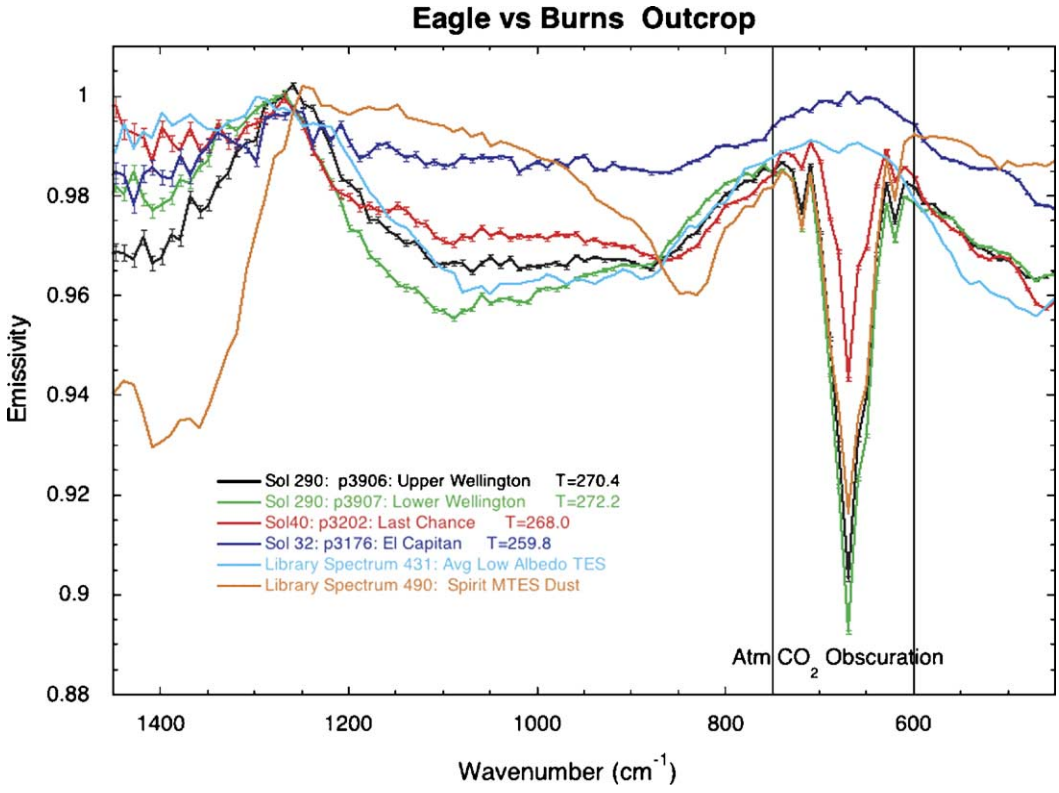

Fig. 18. Comparison of mini-TES spectra for the various units in the Burns formation. Data are shown for the cross-bedded lower unit ("Lower Wellington"), the planar-laminated to low-angle cross-stratified middle unit ("Upper Wellington") in Endurance crater, and the cross-laminated upper unit in Eagle crater ("Last Chance"). Endurance crater observations are plotted in green and black and Eagle crater observations are plotted in blue and red. Note that while the spectral signature at low wavenumbers is nearly the same there are strong differences, especially at wavenumbers above 1000, that suggest compositional variations or changes in the amount of loose sand accumulation across the contact. However, these differences to do not indicate the presence of substantially different mineral contributions. Sulfates are clearly indicated by the strong absorption near 1150 cm^{-1}, and any basaltic contribution would be mostly due to the presence of wind-blown basaltic sand on the surface of the outcrop [4]. The spectra from Burns Cliff (Upper and Lower Wellington) have the highest surface temperatures and strongest bands and likely best represent some of the best spectral signatures of outcrop rocks. For comparison, thin lines show the spectra of average dust signature from the Spirit site and the global dark region from TES in orbit. The spectrum at Last Chance is not as good as shown by its somewhat lower temperature and weaker band depth. Furthermore, the signature of hematite is clearly seen in a peak near 500 cm^{-1}, which indicates that this observation included some surrounding loose concretions and other components of the soil. Spectra of El Capitan are compromised by even lower surface temperatures and higher dust loading in the atmosphere earlier in the mission. This affects the spectral signature by weakening the overall spectral contrast by filling in the absorption features with downwelling sky radiance. This is apparent by the reduced band depth in the silicate absorption at 1000 cm^{-1} and that the atmospheric CO_2 absorption appears weakly in emission. Surface temperatures derived from the observation are noted on the figure. Nearly all the spectra of outcrop rocks in Eagle crater show effects of these kinds. Either the CO_2 band shows in emission rather than absorption (sky contributions and lower surface temperatures) that there are strong hematite features (inclusion of surrounding soils), or in many observations of flat lying rocks the spectra are indistinguishable from that of the average spectral character of dust. Sol number and sequence ID are noted along with the average temperature of the stare. Error bars represent the standard deviation of the mean of 200 or 300 individual scans.

modern terrestrial example of this process is provided by the White Sands playa–dune system of New Mexico [84] and in the Prungle Lakes of southeastern Australia [85], in which sulfate minerals precipitated in a large playa lake during climatic wet periods are reworked during deflation associated with climatically dry periods to form sand dunes made almost entirely of sulfate grains. Groundwater-controlled deflation of playas drives the growth of efflorescent salts within the sediment matrix at the capillary fringe of the saline water-table [86]. If terrigenous sediments are also deposited, then these components also will be included, probably through poikiolitic mineral precipitation, during growth of the crusts. Deflation then drives production of sand-sized aggregates of terrigenous and evaporite minerals [87]. A sustained flux of these aggregate sand grains could be enabled if the rate of deflation balanced crust production for a constant elevation water table, or if the rate of deflation matched the rate of water table lowering [85,87]. Grain production would be optimized if the

capillary fringe was maintained at the sediment–air interface, regardless of the absolute motion of the water table. The production of sulfate-rich sediment particles is characteristic of the arid portions of terrestrial climatic cycles.

6.3. Terrestrial analogs

The essential attributes of the Burns formation which must be explained by any depositional model are: its great lateral extent, for possibly hundreds of kilometers; its dune–interdune facies motif which shows a "wetting upward" trend; and its unusual mineralogy of low-pH sulfate evaporite minerals. On Earth, there is no single analog which can account for this unique set of characteristics. Instead, a hybrid model must be constructed which assimilates specific important characteristics. Some smaller systems come close. For example, playa lakes with pH 2–4 occur in Western Australia, which are apparently precipitating jarosite and alunite, and possibly hematite [88]. However, these lakes are small (<1 km), lack adjacent dune fields, and are not prolific in acid–water mineral production. With regard to acid–water mineral precipitation the Rio Tinto system discussed by Fernandez-Remolar et al. [89] provides a better analog. Here, groundwater oxidation of pyritic ore bodies in the source area of the Río Tinto generates headwaters enriched in sulfuric acid and ferric iron. Evaporation of river water and groundwater drives precipitation of jarosite, schwertmannite, coquimbite, gypsum, and other sulfate minerals [89]. However, the Rio Tinto hydrothermal system does not replicate the dune–interdune/playa setting of the Burns formation and so other, more appropriate physical analogs must be sought.

The Lake Eyre basin, Australia, provides a suitable scale model for the size of the Burns formation depositional system. The preserved aerial extent of the Meridiani hematite deposit–assumed here to provide a constraint on the areal extent of the concretion-bearing Burns formation–is on the order of ~1.5×10^5 km^2 [25]. This is exceeded by the drainage area for the Lake Eyre basin, which is ~1.14×10^6 km^2, but is greater than the area of the active ("Lake Eyre") playa, which has an area of just ~1.0×10^4 km^2; this expanded to ~3.5×10^4 km^2 during the last pluvial period at 125 ka [90,91]. Previously the Lake Eyre basin has been suggested as an analog for parts of the present surface of Mars because of its substantial system size, its arid climate setting, and the presence of fluvial catchments that have morphologic similarity to the incised channel networks on Mars [92]. We support this interpretation and add to it by noting that Lake Eyre itself provides an attractive analog for the ancient Meridiani surface because of its enormous playa surface which lies adjacent to a significant dune field, *supplied with sediment from deflation of the playa surface*. Furthermore, during times of expansion associated with flooding, the lake creates narrow waterways that lace through the interdune network, and these infiltration events may provide good analogs for the overland flow of water indicated by the Burns formation upper unit. These several points of comparison make it a strong analog for the Burns formation. However, the playa deposits were precipitated from normal pH waters, and the playa does not produce significant volumes of evaporite minerals during deflation of the playa surface. Most playa-derived sediments in the adjacent dune field are composed of terrigenous minerals [90].

The White Sands playa–dune system of New Mexico provides an excellent example for understanding how significant production of sulfate eolianites can occur. The source playa provides enough sediment to form a continuous cover of almost pure sulfate sand dunes [93,94]. Sulfate grains are supplied by two processes. In the first case, during wet periods, the playa may fill with water, which subsequently evaporates to form layers of sulfate sediment, including gypsum crystals which disintegrate to form sand-sized grains. In the second case, during dryer periods, the lake may be dry but the groundwater table may stay close enough to the surface so that the capillary fringe wicks salty water to the surface where it dries and precipitates its salts as an efflorescent crust. As the crust alternately wets and dries, it accretes and then breaks down to form sand and silt-sized grains which consist of mineral aggregates. Grains derived from either process are then blown off the playa surface to accumulate as a broad, areally extensive network of dunes and sand sheets (Fig. 9e). The transition from playa to dune field is marked by a zone of dome dunes that give way to transverse and barchan forms in the downwind direction [93,94]. Because the sand is almost entirely of evaporitic, local origin it is texturally immature despite its high susceptibility to mechanical erosion during transport. Sand grains are angular to subrounded and relatively coarse grained. The most source-proximal sands are medium to coarse grained, tapering off to fine to medium grain size for the most distal dunes. Thus, the relative coarse grain size of the Burns formation (Fig. 7a) can be interpreted in light of this distribution to result from the influence of a very local source.

White Sands also provides an important analog for the diagenetic history of the Burns formation, discussed

further by McLennan et al. [7]. The high solubility of these sands results in more extensive early diagenesis than is found in texturally similar but compositionally different quartz-dominated sand dunes at [79,80,93]. At White Sands, diagenesis of the eolian and interdune sulfate sands is largely controlled by the relationship between sand location and the water table [80]. Active sand dunes are in the vadose zone, whereas the interdune sands are in the capillary-fringe and phreatic zones. Infiltration of undersaturated water results in crytallographically controlled dissolution of sulfate grains. In contrast, percolation of evaporatively concentrated groundwater through the capillary-fringe and phreatic zones results in extensive early cementation, forming grain overgrowths and rim cements, in addition to occlusion of entire pore networks.

6.4. Stratigraphic model

On Earth, hydrologically closed basins are very sensitive to fluctuations in climate, which controls the composition of sediments deposited in those basins [95] and their stratigraphic architecture [32,38,63]. Changes in climate lead to variability in surface runoff and fluctuations in water-table elevation. Surface runoff directly affects sedimentation patterns, whereas changes in the elevation of the groundwater table serve mostly to affect the preservation of eolian strata. The exceptions to this are when the capillary zone reaches the surface to induce the formation of crusts, or when the water table rises fully above the surface to form a lake. The stratigraphic architecture of the Burns formation preserves a rich record of interactions between eolian and fluvial (possibly lacustrine) processes, which controlled transport and deposition, and water-table fluctuations, which controlled preservation of strata and diagenesis.

It is possible that the Burns upper unit records a flooding event that was decoupled from variations in the water table. Indeed, there is much evidence on the surface of Mars to suggest episodes of catastrophic release of water [9,96]. Accordingly, similar events may have flooded the plains of Meridiani to create interdune/playa sedimentation. However, this interpretation is not favored due to the lack of evidence for rapid flooding, including the lack of significant erosion at the base of subaqueous deposits, the lack of evidence for high-velocity flows in those deposits, and the lack of evidence for slumping in underlying eolian deposits. These responses to rapid flooding of terrestrial dune fields have been well documented [81–83,97] and are not observed in the Burns formation.

Therefore, the Burns formation is interpreted to record wetting of the Martian surface, very likely related to a relative rise in the water table. Fig. 19 shows one possible scenario involving gradual rise and fall of the groundwater table. This interpretation is based on the stratigraphic succession of facies relative to the position of the Wellington deflation surface, which echoes the

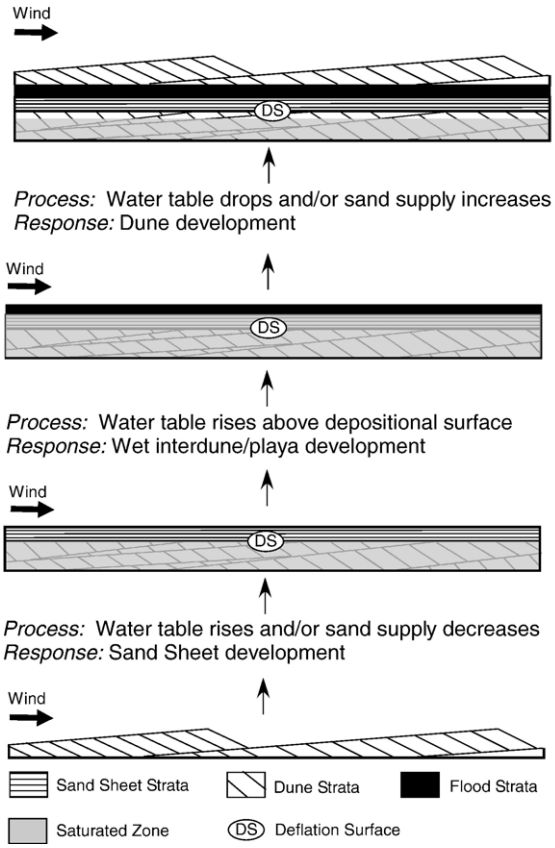

Fig. 19. Depositional model for Burns formation. This model allows for the possibility of regional variations in the groundwater table, on the order of many tens of kilometers. The lower unit of the Burns formation accumulates through the migration of sulfate-rich sand dunes to form large scale cross-bedding. A rise in the water table or a decrease in the flux of wind-blown sand results in the preservation of only part of the dune field, due to limited infiltration by the water table. A deflation surface forms as sediment is removed down to the level of the capillary fringe of the water table. Renewed sand deposition above the capillary fringe results in the development of a sand sheet, but not dune development. Continued rise of the water table results in it breaching the surface to form damp to wet interdune deposits. If the water table is sustained above the depositional surface, then lacustrine deposits may accumulate, which so far have not been observed in the Burns formation. In any event, a subsequent drop in the water table or increase in the flux of wind blown sand predicts development of a younger phase of dune development. Repeated cycles of relative water table rise and fall predict development of stacked dune–interdune facies, which can be tested if thicker sections of strata are discovered, possibly at Victoria crater.

classic patterns preserved in terrestrial eolian sequences that record water-table rise [63,66,78]. As discussed above, the Burns upper unit records damp to wet interdune conditions, and preservation of wet interdune facies in the rock record requires that sediments accumulate as the water table rises and as dunes migrate downwind. The rise can be absolute, perhaps associated with climate change, or relative, due to subsidence of the sediment column through a fixed water table [63].

Other scenarios to explain Burns stratigraphy also are possible, but necessarily involve additional complexity. For example, the Burns might record multiple events of water table oscillation, perhaps superimposed on a longer-term trend toward increasing wetness at the surface. Such additional complexity might be indicated by the dark bands at and above the Whatanga contact, which could represent superimposed episodes of stagnation between events of water table rise and fall. Such a scenario might be supported by the sequence of diagenetic events recorded in the Burns formation [7], which too could be interpreted to record multiple episodes of groundwater oscillation.

6.5. Closing comments

The involvement of liquid water in the origin and diagenesis of the Burns formation is demonstrated by several processes. Liquid water was critically important in forming sediment particles, even in entirely eolian facies; it was locally important in transporting these particles in shallow, overland flows; it was most likely responsible for regulating the stratigraphic architecture of the Burns formation itself; and it was critically important in stimulating several temporally independent diagenetic reactions. The foregoing discussion makes clear the essential role of terrestrial analogs in helping to interpret these past processes on Mars, in much the same way that understanding modern terrestrial processes has helped to provide insight into the ancient history of Earth. The lessons learned from studies of the early Earth underscore one important point, however, that analogs are meant to light the way but are not lamp posts to be leaned on. In avoiding the literal application of uniformitarianism, we have learned to recognize unique processes and environments that characterized the early Earth. In the same sense, we must accept that Earth may not provide suitable analogs for possibly unique Martian processes. Nevertheless, the sedimentology and stratigraphy of the Burns formation are so similar to terrestrial rocks, in many aspects, that the role of unique or even substantially different processes in the development of these particular Martian rocks is not required.

The terrestrial processes outlined above form a null hypothesis for the origin of the Burns formation which can be tested with further study. The first significant test of this hypothesis may occur at Victoria crater (~1 km diameter), about 5 km south of Endurance crater (<200 m diameter). MOLA and MOC data indicate that up to several tens of meters of stratigraphic thickness are exposed in the walls of Victoria crater. If so, then this will provide an excellent opportunity to further interrogate the model presented here for accumulation of the Burns formation, through the search for attributes which do not fit the predictions of terrestrial dune–interdune successions.

Acknowledgements

We gratefully acknowledge the entire science and engineering teams on MER for making this investigation possible. We are also thankful for very helpful discussions on eolian, fluvial, and evaporite sedimentology with Steve Fryberger, Lawrie Hardie, Doug Jerolmack, Gary Kocurek, David Mohrig, Dave Rubin, and John Southard. Steve Fryberger, Gary Kocurek, Dave Rubin, and John Southard provided very helpful reviews of the final manuscript. The National Aeronautics and Space Administration funded the overall MER project and the APXS and Mossauer instruments were funded by the German space agency.

References

[1] M.C. Malin, K.S. Edgett, Sedimentary rocks of early Mars, Science 290 (5498) (2000) 1927–1937.

[2] M.C. Malin, K.S. Edgett, Evidence for persistent flow and aqueous sedimentation on early Mars, Science 302 (5652) (2003) 1931–1934.

[3] S.W. Squyres, J.P. Grotzinger, R.E. Arvidson, J.F. Bell III, W. Calvin, P.R. Christensen, B.C. Clark, J.A. Crisp, W.H. Farrand, K.E. Herkenhoff, J.R. Johnson, G. Klingelhofer, A.H. Knoll, S.M. McLennan, H.Y. McSween Jr., R.V. Morris, J.W. Rice Jr., R. Rieder, L.A. Soderblom, In situ evidence for an ancient aqueous environment at Meridiani Planum, Mars, Science 306 (5702) (2004) 1709–1714.

[4] P.R. Christensen, M.B. Wyatt, T.D. Glotch, A.D. Rogers, S. Anwar, R.E. Arvidson, J.L. Bandfield, D.L. Blaney, C. Budney, W.M. Calvin, A. Fallacaro, R.L. Fergason, N. Gorelick, T.G. Graff, V.E. Hamilton, A.G. Hayes, J.R. Johnson, A.T. Knudson, H.Y. McSween Jr., G.L. Mehall, L.K. Mehall, J.E. Moersch, R.V. Morris, M.D. Smith, S.W. Squyres, S.W. Ruff, M.J. Wolff, Mineralogy at Meridiani Planum from the Mini-TES experiment on the opportunity rover, Science 306 (5702) (2004) 1733–1739.

[5] G. Klingelhofer, R.V. Morris, B. Bernhardt, C. Schroder, D.S. Rodionov, P.A. de Souza Jr., A. Yen, R. Gellert, E.N. Evlanov, B. Zubkov, J. Foh, U. Bonnes, E. Kankeleit, P. Gutlich, D.W. Ming,

F. Renz, T. Wdowiak, S.W. Squyres, R.E. Arvidson, Jarosite and Hematite at Meridiani Planum from opportunity's Mossbauer Spectrometer, Science 306 (5702) (2004) 1740–1745.
[6] R. Rieder, R. Gellert, R.C. Anderson, J. Bruckner, B.C. Clark, G. Dreibus, T. Economou, G. Klingelhöfer, G.W. Lugmair, D.W. Ming, S.W. Squyres, C. d'Uston, H. Wanke, A. Yen, J. Zipfel, Chemistry of rocks and soils at Meridiani Planum from the alpha particle X-ray Spectrometer, Science 306 (5702) (2004) 1746–1749.
[7] S.M. McLennan, J.F. Bell III, W.M. Calvin, P.R. Christensen, B.C. Clark, P.A. de Souza, J. Farmer, W.H. Farrand, D. Fike, R. Gellert, A. Ghosh, T.D. Glotch, J.P. Grotzinger, B. Hahn, K.E. Herkenhoff, J.A. Hurowitz, J.R. Johnson, S.S. Johnson, B. Jolliff, G. Klingelhoffer, A.H. Knoll, Z. Learner, M.C. Malin, H.Y. McSween Jr., J. Pocock, S.W. Ruff, S.W. Squyres, N.J. Tosca, W.A. Watters, M.B. Wyatt, A. Yen, Provenance and diagenesis of the Burns formation, Meridiani Planum, Mars, Earth Planet. Sci. Lett. 240 (2005) 95–121, doi:10.1016/j.epsl.2005.09.038 (this issue).
[8] B.C. Clark, R.V. Morris, S.M. McLennan, R. Gellert, B. Jolliff, A.H. Knoll, S.W. Squyres, T.K. Lowenstein, D.W. Ming, N.J. Tosca, A. Yen, P.R. Christensen, S.P. Gorevan, J. Brückner, W.M. Calvin, G. Dreibus, W.H. Farrand, G. Klingelhöfer, H. Waenke, J. Zipfel, J.F. Bell III, J.P. Grotzinger, H.Y. McSween Jr., R. Rieder, Chemistry and mineralogy of outcrops at Meridiani Planum, Earth Planet. Sci. Lett. 240 (2005) 73–94, doi:10.1016/j.epsl.2005.09.040 (this issue).
[9] P. Masson, M.H. Carr, F. Costard, R. Greeley, E. Hauber, R. Jaumann, Geomorphologic evidence for liquid water, Space Sci. Rev. 96 (1–4) (2001) 333–364.
[10] A.H. Knoll, M.H. Carr, B.C. Clark, D.J. Des Marais, J.D. Farmer, W.W. Fischer, J.P. Grotzinger, A. Hayes, S.M. McLennan, M. Malin, C. Schröder, S.W. Squyres, N.J. Tosca, T. Wdowiak, An astrobiological perspective on Meridiani Planum, Earth Planet. Sci. Lett. 240 (2005) 179–189, doi:10.1016/j.epsl.2005.09.045 (this issue).
[11] N. Christie-Blick, N.W. Driscoll, Sequence stratigraphy, Annu. Rev. Earth Planet. Sci. 23 (1995) 451–478.
[12] P.B. Flemings, J.P. Grotzinger, STRATA: freeware for analyzing classic stratigraphy problems, GSA Today 6 (12) (1996) 1–7.
[13] P.R. Christensen, J.L. Bandfield, R.N. Clark, K.S. Edgett, V.E. Hamilton, T. Hoefen, H.H. Kieffer, R.O. Kuzmin, M.D. Lane, M.C. Malin, R.V. Morris, J.C. Pearl, R. Pearson, T.L. Roush, S.W. Ruff, M.D. Smith, Detection of crystalline hematite mineralization on Mars by the Thermal Emission Spectrometer: evidence for near-surface water, J. Geophys. Res.-Planets 105 (E4) (2000) 9623–9642.
[14] P.R. Christensen, R.V. Morris, M.D. Lane, J.L. Bandfield, M.C. Malin, Global mapping of Martian hematite mineral deposits: remnants of water-driven processes on early Mars, J. Geophys. Res.-Planets 106 (E10) (2001) 23873–23885.
[15] D.H. Scott, K.L. Tanaka, Geologic Map of the Western Equatorial Region of Mars, United States Geological Survey, Denver, 1986.
[16] R. Greeley, J.E. Guest, Geologic Map of the Eastern Equatorial Region of Mars, United States Geological Survey, Denver, 1987.
[17] R.E. Arvidson, F.P. Seelos, K.S. Deal, W.C. Koeppen, N.O. Snider, J.M. Kieniewicz, B.M. Hynek, M.T. Mellon, J.B. Garvin, Mantled and exhumed terrains in Terra Meridiani, Mars, J. Geophys. Res.-Planets 108 (E12) (2003) E8073–E8077.
[18] P.H. Schultz, A.B. Lutz, Polar wandering on Mars, Icarus 73 (1988) 91–141.
[19] K.S. Edgett, T.J. Parker, Water on early Mars: possible subaqueous sedimentary deposits covering ancient cratered terrain in western Arabia and Sinus Meridiani, Geophys. Res. Lett. 24 (22) (1997) 2897–2900.
[20] M. Malin, K.S. Edgett, Mars Global Surveyor Mars Orbiter Camera: interplanetary cruise through primary mission, J. Geophys. Res.-Planets 106 (2001) (2004) E23429–E23570.
[21] L.A. Soderblom, R.C. Anderson, R.E. Arvidson, J.F. Bell III, N.A. Cabrol, W. Calvin, P.R. Christensen, B.C. Clark, T. Economou, B.L. Ehlmann, W.H. Farrand, D. Fike, R. Gellert, T.D. Glotch, M.P. Golombek, R. Greeley, J.P. Grotzinger, K.E. Herkenhoff, D.J. Jerolmack, J.R. Johnson, B. Jolliff, G. Klingelhöfer, A.H. Knoll, Z.A. Learner, R. Li, M.C. Malin, S.M. McLennan, H.Y. McSween, D.W. Ming, R.V. Morris, J.W. Rice Jr., L. Richter, R. Rieder, D. Rodionov, C Schröder, F.P. Seelos IV, J.M. Soderblom, S.W. Squyres, R. Sullivan, W.A. Watters, C.M. Weitz, M.B. Wyatt, A. Yen, J. Zipfel, Soils of eagle crater and Meridiani Planum at the Opportunity rover landing site, Science 306 (5702) (2004) 1723–1726.
[22] M.A. Chan, B. Beitler, W.T. Parry, J. Orno, G. Komatsu, A possible terrestrial analogue for haematite concretions on Mars, Nature 429 (2004) 731–734.
[23] K.S. Edgett, M.C. Malin, Martian sedimentary rock stratigraphy: outcrops and interbedded craters of northwest Sinus Meridiani and southwest Arabia Terra, Geophys. Res. Lett. 29 (32) (2002) 1–4.
[24] R.G. Burns, Ferric sulfates on Mars, J. Geophys. Res.-Planets 92 (1987) E570–E574.
[25] P.R. Christensen, S.W. Ruff, Formation of the hematite-bearing unit in Meridiani Planum: evidence for deposition in standing water, J. Geophys. Res.-Planets 109 (E8) (2004).
[26] R.E. Hunter, Basic types of stratification in small eolian dunes, Sedimentology 24 (1977) 361–387.
[27] D.M. Rubin, R.E. Hunter, Bedform climbing in theory and nature, Sedimentology 29 (1) (1982) 121–138.
[28] S.G. Fryberger, C.J. Schenk, Pin stripe lamination: a distinctive feature of modern and ancient eolian sediments, Sediment. Geol. 55 (1988) 1–55.
[29] J.B. Southard, Representation of bed configuration in depth–velocity–size diagrams, J. Sediment. Petrol. 41 (1973) 903–915.
[30] D.M. Rubin, R.E. Hunter, Reconstructing bedform assemblages from compound crossbedding, in: T.S. Ahlbrandt (Ed.), Aeolian Sediments and Processes, vol. 38, Elsevier, Amsterdam, 1983, pp. 407–428.
[31] R.E. Hunter, D.M. Rubin, Interpreting cyclic crossbedding, with an example from the Navajo Sandstone, in: T.S. Ahlbrandt (Ed.), Aeolian Sediments and Processes, 38, Elsevier, Amsterdam, 1983, pp. 429–454.
[32] M.E. Brookfield, Origin of bounding surfaces in ancient aeolian sandstones, Sedimentology 24 (3) (1977) 303–332.
[33] D.M. Rubin, R.E. Hunter, Field guide to sedimentary structures in the Navajo and Entrada Sandstones in southern Utah and northern Arizona: geologic diversity of Arizona and its margins—excursions to choice areas: Geological Society of America 100th Annual Meeting, Phoenix, Arizona, guidebook, in: E.M. Vanden Dolder (Ed.), Geological Survey Branch Special Paper, vol. 5, Arizona Bureau of Geology and Mineral Technology, 1987, pp. 126–139.
[34] A.D. Miall, Alluvial deposits, in: R.G. Walker, N.P. James (Eds.), Facies Models, Geological Association of Canada, St. John's, 1992, pp. 119–142.

[35] R.W. Dalrymple, Tidal depositional systems, in: R.G. Walker, N.P. James (Eds.), Facies Models, Geological Association of Canada, St. John's, 1992, pp. 195–218.
[36] F.D. Stacey, Physics of the Earth, Brookfield Press, Kenmore, 1992, 519 pp.
[37] I. de Pater, J.J. Lissauer, Planetary Sciences, Cambridge Univ. Press, Cambridge, 2001, 568 pp.
[38] T.S. Ahlbrandt, S.G. Fryberger, in: Introduction to Eolian Deposits: Siliciclastic Environments Memoir, vol. X, American Association of Petroleum Geologists, Tulsa, 1981, pp. 11–47.
[39] R.E. Hunter, Terminology of cross-stratified sedimentary layers and climbing-ripple structures, J. Sediment. Petrol. 47 (2) (1977) 697–706.
[40] S.G. Fryberger, G. Dean, E.D. McKee, Dune forms and wind regime, in: E.D. McKee (Ed.), A Study of Global Sand Seas, Professional Paper, vol. 1052, U. S. Geological Survey, Denver, 1979, pp. 137–170.
[41] G. Kocurek, J. Nielson, Conditions favourable for the formation of warm-climate aeolian sand sheets, Sedimentology 33 (1986) 795–816.
[42] T.S. Ahlbrandt, S.G. Fryberger, Sedimentary features and significance of interdune deposits, in: R.M. Flores (Ed.), Recent and Ancient Non-Marine Depositional Environments: Models for Exploration, Special Publication, vol. 31, Society of Economic Mineralogists and Paleontologists, Tulsa, 1981, pp. 293–314.
[43] D.J.J. Kinsman, Modes of formation, sedimentary associations, and diagnostic features of shallow water and supratidal evaporites, Am. Assoc. Petrol. Geol. Bull. 53 (1969) 830–840.
[44] G. Kocurek, Significance of interdune deposits and bounding surfaces in aeolian dune sands, Sedimentology 28 (6) (1981) 753–780.
[45] M.E. Sanz, J.P. Rodríguez-Aranda, J.P. Calvo, S. Ordónez, Tertiary detrital gypsum in the Madrid Basin, Spain: criteria for interpreting detrital gypsum in continental evaporitic sequences, in: W.M. Last (Ed.), Sedimentology and Geochemistry of Modern and Ancient Saline Lakes, Special Publication, vol. 50, Society of Economic Mineralogists and Paleontologists, Tulsa, 1994, pp. 217–228.
[46] D.M. Rubin, Cross-bedding, Bedforms, and Paleocurrents, Society of Economic Paleontologists and Mineralogists, Tulsa, 1987, 187 pp.
[47] G.M. Ashley, J.B. Southard, J.C. Boothroyd, Deposition of climbing-ripple beds: a flume simulation, Sedimentology 29 (1) (1982) 67–79.
[48] J.C. Harms, J.B. Southard, D.R. Spearing, R.G. Walker, Depositional Environments as Interpreted From Primary Sedimentary Structures and Stratification Sequences, Society of Economic Mineralogists and Paleontologists, Tulsa, 1975, 161 pp.
[49] J.C. Harms, J.B. Southard, R.G. Walker, Structures and Sequences in Clastic Rocks, Society of Economic Mineralogists and Paleontologists, Tulsa, 1982, 253 pp.
[50] G.V. Middleton, J.B. Southard, Mechanics of Sediment Movement, Society of Economic Mineralogists and Paleontologists, Tulsa, 1984, 401 pp.
[51] R.E. Hunter, Subaqueous sand-flow cross strata, J. Sediment. Petrol. 55 (6) (1985) 886–894.
[52] J.B. Southard, L.A. Boguchwal, Bed configurations in steady unidirectional flows: Part 3. Effects of temperature and gravity, J. Sediment. Petrol. 60 (1990) 680–686.
[53] R.P. Sharp, Wind ripples, J. Geol. 71 (5) (1963) 617–636.
[54] D.M. Rubin, Personal Communication, 2004.
[55] R. Greeley, J. Iverson, Wind as a Geological Process on Earth, Mars, Venus and Titan, Cambridge Univ. Press, New York, 1985.
[56] R. Greeley, S.W. Squyres, R.E. Arvidson, P. Bartlett, J.F. Bell, D. Blaney, N.A. Cabrol, J. Farmer, B. Farrand, M.P. Golombek, S.P. Gorevan, J.A. Grant, A.F.C. Haldemann, K.E. Herkenhoff, J. Johnson, G. Landis, M.B. Madsen, S.M. McLennan, J. Moersch, J.W. Rice, L. Richter, S. Ruff, R.J. Sullivan, S.D. Thompson, A. Wang, C.M. Weitz, P. Whelley, Wind-related processes detected by the Spirit rover at Gusev Crater, Mars, Science 305 (5685) (2004) 810–813.
[57] R. Sullivan, et al., Aeolian processes at the Mars Exploration Rover Meridiani Planum landing site, Nature 436 (2005) 58–61.
[58] R.P. Sharp, M.C. Malin, Surface geology from Viking Landers on Mars: a second look, Geol. Soc. Am. Bull. 95 (12) (1984) 1398–1412.
[59] R. Greeley, M. Kraft, R. Sullivan, G. Wilson, N. Bridges, K. Herkenhoff, R.O. Kuzmin, M. Malin, W. Ward, Aeolian features and processes at the Mars Pathfinder landing site, J. Geophys. Res.-Planets 104 (E9) (1999) 22065.
[60] J.B. Southard, L.A. Boguchwal, Bed configurations in steady unidirectional flows: Part 2. Synthesis of flume data, J. Sediment. Petrol. 60 (1990) 658–679.
[61] L.A. Boguchwal, J.B. Southard, Bed configurations in steady unidirectional flows: Part 1. Scale model using fine sands, J. Sediment. Petrol. 60 (1990) 649–657.
[62] S.G. Fryberger, T.S. Ahlbrandt, S. Andrews, Origin, sedimentary features, and significance of low-angle eolian "sand sheet" deposits, Great Sand Dunes National Monument and vicinity, Colorado, J. Sediment. Petrol. 49 (1979) 733–746.
[63] G. Kocurek, K.G. Havholm, Eolian sequence stratigraphy—a conceptual framework, in: H.W. Posamentier (Ed.), Siliciclastic Sequence Stratigraphy, Memoir, vol. 58, American Association of Petroleum Geologists, Tulsa, OK, 1993, pp. 393–409.
[64] M. Crabaugh, G. Kocurek, The dynamics and environmental context of aeolian sedimentary systems, in: K.e. Pye (Ed.), International Symposium on Aeolian Sedimentary Systems, vol. 72, London, United Kingdom, 1993, pp. 103–126.
[65] K.G. Havholm, R.C. Blakey, M. Capps, L.S. Jones, D.D. King, G. Kocurek, Aeolian genetic stratigraphy: an example from the Middle Jurassic Page Sandstone, Colorado Plateau, in: N. Lancaster (Ed.), Aeolian Sediments: Ancient and Modern, vol. 16, Blackwell Scientific Publications, Oxford, 1993, pp. 87–107.
[66] N.P. Mountney, D.B. Thompson, Stratigraphic evolution and preservation of aeolian dune and damp/wet interdune strata: an example from the Triassic Helsby Sandstone Formation, Cheshire Basin, UK, Sedimentology 49 (4) (2002) 805–833.
[67] R.E. Hunter, Stratification styles in eolian sandstones: some Pennsylvanian to Jurassic examples from the Western Interior U.S.A., in: R.M. Flores (Ed.), Recent and Ancient Nonmarine Depositional Environments: Models for Exploration, Special Publication, vol. 31, SEPM, Tulsa, OK, 1981, pp. 315–329.
[68] S.G. Fryberger, M.A.-S. Abdulkader, T.J. Clisham, Eolian dune, interdune, sand sheet, and siliciclastic sabkha sediments of an offshore-prograding sand sea, Dhahran area, Saudi Arabia, Am. Assoc. Petrol. Geol. Bull. 67 (1983) 280–312.
[69] P.M. Sadler, Sediment accumulation rates and the completeness of the stratigraphic record, J. Geol. 89 (1981) 569–584.
[70] R. Slingerland, J.W. Harbaugh, K.P. Furlong, Simulating Clastic Sedimentary Basins, PTR Prentice Hall Sedimentary Geology Series, Prentice-Hall, Englewood Cliffs, NJ, 1994, p. 220.

[71] C. Paola, J. Mullin, C. Ellis, D.C. Mohrig, J.B. Swenson, G.S. Parker, T. Hickson, P.L. Heller, L. Pratson, J. Syvitski, B. Sheets, N. Strong, Experimental stratigraphy, GSA Today 11 (7) (2001) 4–9.
[72] E. Blackwelder, The valuation of unconformities, J. Geol. 27 (1909) 289–299.
[73] J. Barrell, Rhythms and the measurements of geologic time, Geol. Soc. Am. Bull. 28 (1917) 745–904.
[74] H.E. Wheeler, Stratigraphic units in time and space, Am. J. Sci. 257 (10) (1959) 692–706.
[75] L.L. Sloss, Sequences in the cratonic interior of North America, Geol. Soc. Am. Bull. 74 (2) (1963) 93–113.
[76] P.R. Vail, R.M. Mitchum Jr., S. Thompson III, Seismic stratigraphy and global changes of sea level: Part 3. Relative changes of sea level from coastal onlap, in: C.E.E. Payton (Ed.), Seismic Stratigraphy; Applications to Hydrocarbon Exploration, Memoir, 26, American Association of Petroleum Geologists, Tulsa, 1977, pp. 63–81.
[77] W.L. Stokes, Multiple parallel-truncation bedding planes—a feature of wind-deposited sandstone formations, J. Sediment. Petrol. 38 (2) (1968) 510–515.
[78] S.G. Fryberger, C.J. Schenk, L.F. Krystinik, Stokes surfaces and the effects of near-surface groundwater-table on aeolian deposition, Sedimentology 35 (1) (1988) 21–41.
[79] E.L. Simpson, D.B. Loope, Amalgamated interdune deposits, White-Sands, New-Mexico, J. Sediment. Petrol. 55 (3) (1985) 361–365.
[80] C.J. Schenk, S.G. Fryberger, Early diagenesis of eolian dune and interdune sands at White Sands, New-Mexico, Sediment. Geol. 55 (1988) 109–120.
[81] A. Stromback, J. Howell, Distribution and reservoir properties of the soft sediment deformed Weissliegend the UK, Southern North Sea, Petrol. Geosci. 8 (2002) 237–249.
[82] T.B. Eschner, G. Kocurek, Origins of relief along contacts between eolian sandstones and overlying marine strata, Am. Assoc. Petrol. Geol. Bull. 72 (8) (1988) 932–943.
[83] S.G. Fryberger, L.F. Krystinik, C.J. Schenk, Tidally flooded back-barrier dunefield, Guerrero Negro Area, Baja California, Mexico, Sedimentology 37 (1) (1990) 23–43.
[84] R.P. Langford, The Holocene history of the White Sands dune field and influences on eolian deflation and playa lakes, Quat. Int. 104 (2003) 31–39.
[85] J.W. Magee, Late Quaternary lacustrine, groundwater, aeolian and pedogenic gypsum in the Prungle Lakes, Southeastern Australia, Palaeogeogr. Palaeoclimatol. Palaeoecol. 84 (1–4) (1991) 3–42.
[86] A. Watson, Structure, chemistry and origins of gypsum crusts in Southern Tunisia and the Central Namib-Desert, Sedimentology 32 (6) (1985) 855–875.
[87] J.M. Bowler, Clay dunes: their occurrence, formation, and environmental significance, Earth Sci. Rev. 12 (1973) 315–338.
[88] K.C. Benison, D.A. Laclair, Modern and ancient extremely acid saline deposits: terrestrial Analogs for Martian Environments? Astrobiology 3 (2003) 609–618.
[89] D.C. Fernández-Remolar, R.V. Morris, J.E. Gruener, R. Amils, A.H. Knoll, The Río Tinto Basin, Spain: Mineralogy, Sedimentary Geobiology, and Implications for Interpretation of Outcrop Rocks at Meridiani Planum, Mars, Earth Planet. Sci. Lett. 240 (2005) 149–167, doi:10.1016/j.epsl.2005.09.043 (this issue).
[90] G.C. Nanson, R.A. Callen, D.M. Price, Hydroclimatic interpretation of Quaternary shorelines on south Australian playas, Palaeogeogr. Palaeoclimatol. Palaeoecol. 144 (3–4) (1998) 281–305.
[91] S.B. DeVogel, J.W. Magee, W.F. Manley, G.H. Miller, A GIS-based reconstruction of late Quaternary paleohydrology: Lake Eyre, arid central Australia, Palaeogeogr. Palaeoclimatol. Palaeoecol. 204 (2004) 1–13.
[92] M.C. Bourke, J.R. Zimbelman, Australian paleoflood systems: an analogue for Martian channel systems, Proceedings of the XXXI Lunar and Planetary Science Conference 31 Houston, 2000, p. 1393.
[93] E.D. McKee, Structures of dunes at White Sands National Monument, New Mexico (and a comparison with structures of dunes from other selected areas), Sedimentology 7 (1) (1966) 1–69.
[94] E.D. McKee, R.J. Moiola, Geometry and growth of White Sands Dune Field, New-Mexico, J. Res. U.S. Geol. Surv. 3 (1) (1975) 59–66.
[95] H.P. Eugster, Climatic significance of lake and evaporite deposits, Climate in Earth history, Studies in Geophysics, National Academy Press, Washington, DC, 1982, pp. 105–111.
[96] M.H. Carr, Water on Mars, Oxford Univ. Press, New York, 1996, 299 pp.
[97] K.W. Glennie, A.T. Buller, The Permian Weissliegendes of N.W. Europe: the partial deformation of aeolian dune sands caused by the Zechstein transgression, Sediment. Geol. 35 (1) (1983) 43–81.
[98] D. Winston, Fluvial systems of the Precambrian Belt Supergroup, Montana and Idaho, U.S.A, in: A.D. Mial (Ed.), Fluvial Sedimentology, Memoir, vol. 5, Canadian Society of Petroleum Geologists, Calgary, 1978, pp. 343–359.